Chapter 1
Selected Challenges in Realistic Multibody Modeling of Machines and Vehicles

Jorge Ambrósio

Abstract Multibody modelling involves taking fundamental decisions during the multibody model construction that not only condition its validity for the particular application foreseen but also have fundamental implications on the suitability of the numerical methods used on its analysis. The decision on allowing a particular flexible body to exhibit linear or nonlinear deformations or even to consider it part of the multibody system or as a structural component with which the system interacts is a crucial part of the modeling process. The description of the kinematic relations between moving components can be represented by perfect kinematic constraints or by contact pairs, as when local effects in the joints, generally associated with deviations from nominal conditions or to functional features, must be considered. The interaction of the multibody model with the 'environment' may require a substantial modelling effort that involves decisions on geometric description of features, on contact mechanics or even on numerical methodologies to handle co-simulation of systems with equilibrium equations that are solved with different numerical methods. Several areas are transversal to all the challenges identified and discussed here. The suitability of the numerical time integrators not only to handle the multibody model assumptions but also their interaction with other systems are of fundamental importance in the correct solution of the system dynamics. Descriptive and differential geometry also plays a very important role not only in the description of the relative kinematics of the systems but also in the modelling of the interactions.

Keywords Geometry · Look-up-table · Clearance joints · Contact mechanics · Numerical integration

J. Ambrósio (✉)
IDMEC, Instituto Superior Técnico, University of Lisbon, Lisbon, Portugal
e-mail: Jorge.Ambrosio@tecnico.ulisboa.pt

E. Zahariev, J. Cuadrado (eds.), *IUTAM Symposium on Intelligent Multibody Systems – Dynamics, Control, Simulation*, IUTAM Bookseries 33,
https://doi.org/10.1007/978-3-030-00527-6_1

1.1 Introduction

The early developments of multibody dynamics focused the dynamics of spacecrafts, modelled as rigid bodies [1] or the biomechanics of the human body for space applications [2, 3]. Among others, the work of Wittenburg addressed the dynamics of coupled bodies [4] and originated the first software tool based on multibody dynamics methods for simulating the dynamics injury biomechanics in car accidents, the software tool MESA VERDE (MEchanism, SAtellite, VEhicle, Robot Dynamics Equations) [5]. The developments in multibody dynamics continued being reported in important meetings, started by that organized by Magnus [6], in which the term Multibody Dynamics was coined, and followed by the NATO-ASI on computer-aided analysis and optimization of multibody systems organized by Haug in 1983 [7], the IUTAM symposium on dynamics of multibody systems organized by Bianchi and Schiehlen in 1985 [8] and the NATO-ASI on multibody dynamics organized by Pereira and Ambrosio in 1993 [9]. In a review of the State-of-Art of multibody dynamics, in 1997, Schiehlen [10] identified most of the formalisms used today, as being developed already. Textbooks published by Wittenburg [11], Nikravesh [12], Kane et al. [13], Haug [14] or Garcia de Jalon and Bayo [15], describe such formalisms in a comprehensive manner. The inspiring applications of multibody dynamics, in particular to vehicle dynamics, general machinery and aerospace, and challenges for new developments, which included data models for CAD, parameter optimization for surrogate models, optimal design of multibody systems, strength analysis, i.e., flexible multibody dynamics, contact/impact problems, mechatronics or multiphysics problems, in which the interaction with fluids posed important challenges, were identified by Schiehlen as challenges for the community to be addressed [10]. Also the numerical issues associated with time integration codes or with real-time simulation were already deemed as challenges for the development of multibody systems at the time [10], and still remain important challenges today.

A major challenge that soon emerged in multibody dynamics involved the deformations of the components of the system. In most of the earlier work dealing with the elastodynamics of mechanical systems the deformations of the system components, assumed elastic and small, is superimposed to their large rigid body motion, as observed in different reviews, Erdman and Sandor [16], Lowen and Chassapis [17] and Thompson and Sung [18]. Using reference frames fixed to planar flexible bodies, Song and Haug [19] suggest a finite element based methodology, which yields coupled gross rigid body motion and small elastic deformations, which is further developed and generalized by Shabana and Wehage [20, 21] that use substructuring and the mode component synthesis to reduce the number of generalized coordinates required to represent the flexible components. The community studying space dynamics was naturally involved in dealing with the dynamics of flexible bodies undergoing large rigid body motion. The problem that attracted their initial attention was the stabilization of spinning spacecrafts with flexible appendages [22]. The need to characterize dynamically and control

such systems, in particular, motivated valuable investigations on flexible multibody dynamic [23, 24]. In the framework of the spinning spacecrafts modeling, Kane, Ryan and Banerjee [25] showed that though most of the flexible multibody methods, at the time, could capture the inertia coupling between the elastodynamics of the system components and their large motion but they would still produce incorrect results because they neglected the dynamic stiffening effects. This comment and the research work, in the years that followed, addressing the nature and the solutions of such problem [26] also fostered the need for more systematic approaches to deal with nonlinear deformations in flexible multibody dynamics. Although the floating reference frame methods used in flexible multibody dynamics have the ability to lower the geometric nonlinearities of the flexible bodies they do not eliminate them because the moderate rotation assumption about the floating reference frame is still required [27]. The work of researchers in the finite element community, such as that by Belytschko and Hsieh [28], Simo and Vu-Quoc [29] or Bathe and Bolourchi [30] among others, addressing the same type of problems dealt with a similar problem. Recognizing the problem posed and using some of the approaches well in line with those of the finite element community Cardona and Geradin proposed formulations for the nonlinear flexible bodies using either a geometrically exact model [31] or through substructuring [32]. Defining it as an absolute nodal coordinate formulation, Shabana [33] used finite rotations nodal coordinates enabling the capture of the geometric nonlinear deformations. Another approach taken by Ambrósio and Nikravesh [34] to model geometrically nonlinear flexible bodies was to relax the need for the structures to exhibit small moderate rotations about the floating frame by using an incremental finite element approach within the flexible body description. The approach is further extended to handle material nonlinearities of flexible multibody systems also [35] which is applied to different types of nonlinear flexible body systems including vehicle crash dynamics [36]. In a review of the State-of-Art in flexible multibody dynamics Shabana [37] identified most of the formalisms to describe flexible bodies used today and presented views on, what were at the time, current and future research directions. The topics on nonlinear deformations of flexible bodies, on the stiff nature of the flexible body equations of motion due to the coexistence of high and low frequency components in the system response, on the use of flexible multibody dynamics in the context of computer graphics or the raise of importance of these tools in the field of biomechanics were some of research directions identified. A good part of the current approaches to flexible multibody dynamics is presented in textbooks such as those by Geradin and Cardona [38], Shabana [20], Bauchau [39] or Bremer [40].

In both rigid and flexible multibody systems the correct representation of the kinematic or kinetic relations between different bodies is of fundamental importance for the identification of the correct system dynamic response. The traditional multibody formalisms handle such relative motion restrictions as kinematic constraints [11–15, 20, 38–40]. The complexity of such kinematic restrictions, or kinematic joints, may be relatively small, as for the most common spherical, revolute or translations joints, or extremely high such as in the case of spatial cam joints, as those studied by Gonzales-Palacios and Angeles [41, 42] or path-follower

constraints used in roller coaster applications, as those proposed by Pombo and Ambrosio [43, 44] or by Tandl and Kecskemethy [45, 46]. In a real mechanical joint a gap is always present, being necessary not only to allow the relative motion between the connected bodies but also to permit the components assemblage. No matter how small the clearance is, it can lead to vibration and fatigue phenomena, wear, and lack of precision or even random overall behavior [47]. However, clearance joints also allow for the use of bushings, fundamental to control the vibration in some systems and to allow small misalignments between connected bodies that, otherwise, would not exhibit the correct mobility [48, 49]. A general formulation for joints with clearance and/or bushing elements, eventually having joint motion stops, was proposed by Ambrosio and Pombo [50]. Using an approach based on non-smooth mechanics Akhadkar et al. also addressed the modelling of clearance joints with efficiency [51]. In the framework of rigid multibody systems a large library of kinematic joints, with or without clearances or bushings, has been developed using the coordinates of choice of the developers. The introduction of flexible bodies in the system involves using new sets of generalized coordinates to describe the flexibility. Even if the finite element method is used to describe the system flexibility, depending on the formulation in flexible multibody dynamics any kinematic joint available in a multibody code must be implemented with the new generalized coordinates if it is to be used in the model construction [52]. If the joint axis, itself, is flexible there is no way around it and it has to be formulated using the set of generalized coordinates involved in the formulation [53, 54]. However, if there are no local deformation effects in the joint itself, except for those associated with bushings, it is advantageous that all library of joints, kinematically perfect or represented by clearance/bushings, can be used without requiring them to be formulated with the new generalized coordinates. The use of virtual bodies, i.e., massless rigid bodies fixed to in the locations of the flexible bodies in which kinematic joints need to be connected, proposed by Bae et al. [55] and further developed by Gonçalves and Ambrosio [56], solves the problem with computational efficiency.

Although some challenges remain in terms of formulation of rigid and flexible multibody systems and on the kinematic or contact description of the joints, the identification of the major challenges has been driven by applications associated to vehicle dynamics, both road and railway, biomechanical systems, mechatronics, spacecrafts or high-precision machinery. Transversal to all areas in which challenges in multibody dynamics are identified is the computational geometry for description of curves and surfaces, required in the formulation of all kinds of interactions involving rigid or flexible bodies. Inheriting part of the framework of their formalisms from the computational geometry, the efficient formulation of complex kinematic joints is highly dependent on the efficient use of the geometric information, being this a challenge to be addressed. Contact mechanics, which always played a very important role in the dynamics of multibody systems, bases its formulations on the correct solution of the contact detection problem, which basically involves comparing geometries. In both kinematics and contact

the requirements for the geometric formulation of the curves and surfaces are highly dependent on the formulations used in their implementation and on the numerical methods used for the solution. In the framework of the formulation of clearance/bushing joints all issues associated with geometry and contact mechanics are inherited and play important roles in the accurate and efficient descriptions. The use of online calculations or of Look-up-Tables (LuT), associated to the geometry of the interacting bodies in the framework of kinematics or contact, may also be determinant for the computational efficiency of a multibody program. These are of particular interest in application in which the surfaces or trajectories are very long over a non-regular geometry, being the information contained in the LuT associated with position, normal and tangent vectors and their derivatives as function of the curve or surface defining parameters, in kinematics or in contact detection, or with reaction forces and moments, in the solution of the contact law in contact mechanics. The implication of the different strategies in dealing with the geometric aspects in the context of multibody dynamics is directly observed in the behavior of the time integrator schemes used for the dynamic analysis. Therefore, the computational geometry challenges associated to kinematic formulation of spatial joints of the path-following type and contact mechanics, are addressed here. In the process, the relation between the requirements for the description of geometric features and the numerical methods used are handled with particular attention.

1.2 Geometry in Multibody Dynamics

Multibody dynamics involves the interaction between bodies, regardless of these being rigid or flexible, described by contact pairs or by restrictions of their relative motion. In order to have a computational efficient description of the body-to-body interaction the description of the geometry of the interacting curves or surfaces has to be computationally efficient, to be smooth, to have the correct degree of continuity and to allow establishing all quantities required to the proper description of the phenomena. The interaction between two bodies can be described by a kinematic constraint, such as those in cams [41], point follower mechanisms [42] or in roller coasters [43, 46]. In this case not only the description of the curve, or surface, geometry, including its normal and tangent vectors, is required but also the derivatives of all these quantities with respect to the parameters used for their description. When the interaction is described as a contact problem, such as in contact/impact between different bodies [57–60], description of biological articular surfaces [61–63] or in the formulation of clearance joints [47–50], the need to higher derivatives of the normal and tangent vectors to the surfaces or curves may not exist. In turn, due to the non-smoothness of the problem, the demand for computational efficiency is extremely high requiring that information on the geometry is properly stored and interpolated or solved online.

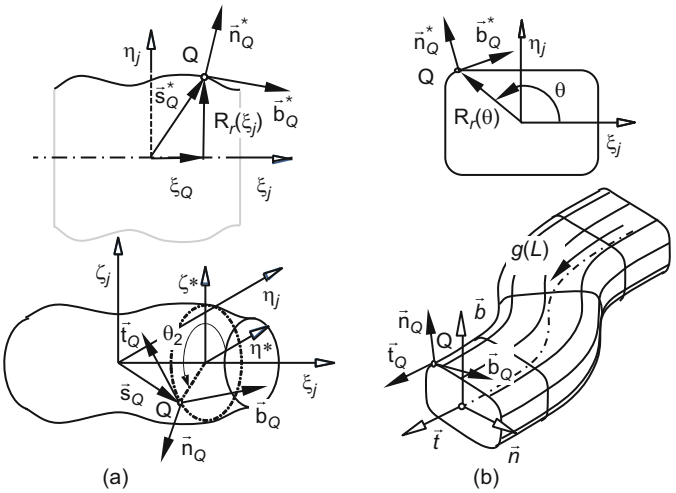

Fig. 1.1 Surfaces resulting from sweeping planar curves about axis or along spatial curves: (**a**) Surface of revolution; (**b**) Extrusion surface

1.2.1 Geometry of Curves and Surfaces

In a wide number of multibody systems bodies surface geometries that result from the sweeping of a cross section around an axis, known as surfaces of revolution, or along a curve, known as extrusions or sweep surfaces, play important roles [64]. Figure 1.1 presents general forms of bodies geometries resulting from sweeping planar curves.

The surface of revolution is obtained by rotating a plane line about an axis of revolution, as in Fig. 1.1a. The coordinates of any point in the surface are expressed in terms of the parameters defining the planar line, $R(\xi_j)$, and the sweep angle, is θ_2. In the $(\xi\eta)_j$ plane the position of point Q is a function of a single parameter, the coordinate ξ_Q, as,

$$\mathbf{s}_Q^* = \begin{Bmatrix} \xi_Q \\ R\left(\xi_Q\right) \\ 0 \end{Bmatrix} \tag{1.1}$$

The normal and tangent vectors to point Q in the line, in Fig. 1.1a, are also functions of the parameter defining the line as,

$$\mathbf{n}_Q^* = \begin{Bmatrix} n_{\xi_Q}^*\left(\xi_Q\right) \\ n_{\eta_Q}^*\left(\xi_Q\right) \\ 0 \end{Bmatrix} \;\; ; \;\; \mathbf{b}_Q^* = \begin{Bmatrix} b_{\xi_Q}^*\left(\xi_Q\right) \\ b_{\eta_Q}^*\left(\xi_Q\right) \\ 0 \end{Bmatrix} \tag{1.2}$$

The surface of revolution is obtained by rotating the line around the axis of revolution ξ_j. This operation is a transformation of coordinates in which any point on the line, given by Eq. (1.1), and the normal and tangent vectors, described in Eq. (1.2), are rotated as,

$$\begin{aligned} \mathbf{s}'_Q &= \mathbf{A}_{\theta_2}\mathbf{s}^*_Q \\ \mathbf{n}'_Q &= \mathbf{A}_{\theta_2}\mathbf{n}^*_Q \\ \mathbf{b}'_Q &= \mathbf{A}_{\theta_2}\mathbf{b}^*_Q \end{aligned} \tag{1.3}$$

in which the rotation matrix $\mathbf{A}_{\theta_2}$ is defined as,

$$\mathbf{A}_{\theta_2} = \begin{bmatrix} 1 & 0 & 0 \\ 0 & \cos\theta_2 & -\sin\theta_2 \\ 0 & \sin\theta_2 & \cos\theta_2 \end{bmatrix} \tag{1.4}$$

The point Q position on the surface of revolution and the vectors associated to the surface, given by Eq. (1.3) are expressed in the body j coordinate system. The tangent to the surface on point Q, $\mathbf{t}'_Q$, is perpendicular to both $\mathbf{n}'_Q$ and $\mathbf{b}'_Q$, being calculated by using the cross product between these vectors.

An extrusion, or sweep, surface is obtained by sweeping a planar line, and eventually rotating it, along a spatial line. Take the line shown in Fig. 1.1b, for which the position of point Q, in the $(\xi\eta)_j$ plane, is a function of a single parameter, θ, being written as,

$$\mathbf{s}^*_Q = R(\theta) \begin{Bmatrix} \cos\theta \\ \sin\theta \\ 0 \end{Bmatrix} \tag{1.5}$$

The normal and tangent vectors to point Q in the line, in Fig. 1.1b, also functions of the parameter defining the line, are written in a generic form as in Eq. (1.2).

Let the curve along which the planar curve is swept, shown in Fig. 1.2b, be defined in body j coordinates as function of an arc-length parameter L. Let a moving coordinate frame, defined by vectors $\mathbf{n}$, $\mathbf{b}$ and $\mathbf{t}$. The position of a point Q in the surface and the corresponding normal and tangent vectors are now written as

$$\begin{aligned} \mathbf{s}'_Q &= \mathbf{g}'(L) + \mathbf{A}_r\mathbf{s}^*_Q \\ \mathbf{n}'_Q &= \mathbf{A}_r\mathbf{n}^*_Q \\ \mathbf{b}'_Q &= \mathbf{A}_r\mathbf{b}^*_Q \end{aligned} \tag{1.6}$$

in which the rotation matrix $\mathbf{A}_r$ is defined as,

$$\mathbf{A}_r = \left[\mathbf{n}'(L) \;\; \mathbf{b}'(L) \;\; \mathbf{t}'(L)\right] \tag{1.7}$$

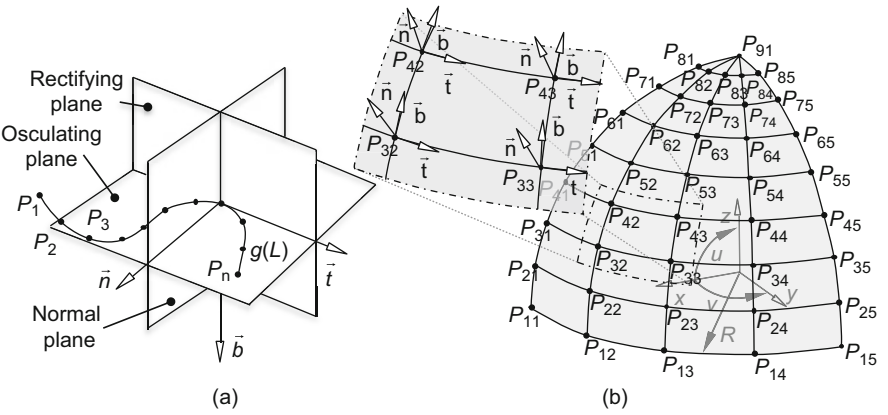

Fig. 1.2 Parametric representations of curves and surfaces: (**a**) Spatial curve; (**b**) Freeform surface

where all vectors are expressed in the body j coordinate system, i.e., in the coordinate system of the body to which the spatial line is attached.

A general form of representing curves and surfaces implies a parametric description in which a single parameter is enough for a curve, for instance parameter L in Fig. 1.2a, and two parameters are necessary for a surface, as parameters u and v for the surface in Fig. 1.2b. Then, the position of the points that belong to the curve, or the surface, and the normal and tangent vectors are explicitly obtained by mappings those parameters into a 3D-space.

The spatial curve be described using an n^{th} order spline segments, interpolating a set of control points, defined as

$$\mathbf{g}(u) = \left\{ \begin{array}{c} x(u) \\ y(u) \\ z(u) \end{array} \right\} = a_0 + a_1 u + a_2 u^2 + a_3 u^3 + \cdots + a_n u^n \tag{1.8}$$

where $\mathbf{g}(u)$ is the vector locating a point on the curve, u is the local parametric variable and a_i are unknown algebraic coefficients that must be calculated using points with known coordinates. The curve moving frame, described by the Frenet frame in this work, the starts with the identification of the osculating plane, at a given point P on a curve, which is the plane of closest contact to the curve in the neighborhood of P [65]. The tangent vector $\mathbf{t}$ and the principal normal vector $\mathbf{n}$ are defined in the osculating plane. The binormal vector $\mathbf{b}$ is defined as being normal to the other two vectors, as shown in Fig. 1.2a. These vectors are defined in the intersection of the normal, rectifying and osculating planes, point P, and can be written as [43]

$$\mathbf{t} = \frac{\mathbf{g}^u}{\|\mathbf{g}^u\|} \; ; \; \mathbf{n} = \frac{\mathbf{k}}{\|\mathbf{k}\|} \; ; \; \mathbf{b} = \tilde{\mathbf{t}}\mathbf{n} \tag{1.9}$$

where $\tilde{\mathbf{t}}\mathbf{n}$ means a cross product and the auxiliary vector $\mathbf{k}$ is given by

$$\mathbf{k} = \mathbf{g}^{uu} - \frac{\mathbf{g}^{uu^T}\mathbf{g}^u}{\|\mathbf{g}^u\|^2}\mathbf{g}^u \tag{1.10}$$

in which $\mathbf{g}^u$ and $\mathbf{g}^{uu}$ are, respectively, the first and second derivatives of the parametric curve $\mathbf{g}(u)$ with respect to the parametric variable u.

The parametric surface, shown in Fig. 1.2b, can be expressed by parameters u and v that map into a 3D space. Without lack of generality, take the example of a spherical cap, which has the parametric representation given by

$$\mathrm{s}(u, v) = \begin{cases} x = R\sqrt{\cos^2 u \cos^2 v} \\ y = R\sqrt{\cos^2 u \sin^2 v} \\ z = R\sqrt{\sin^2 u} \end{cases} \quad \begin{matrix} 0 \le u \le \frac{\pi}{2} \quad [\text{rad}] \\ 0 \le v < \frac{\pi}{2} \quad [\text{rad}] \end{matrix} \tag{1.11}$$

For each point in the surface, tangent vectors to the u and v directions, referred to as tangent and bitangent vectors respectively,

$$\mathbf{t}^u \equiv \mathbf{t}^u(u, v) = \frac{\partial \mathbf{s}(u, v)}{\partial u}, \quad \mathbf{t}^v \equiv \mathrm{t}^v(u, v) = \frac{\partial \mathbf{s}(u, v)}{\partial v} \tag{1.12}$$

$$\mathbf{n} \equiv \mathbf{n}(u, v) = \frac{\tilde{\mathbf{t}}^u \mathbf{t}^v}{\left\|\tilde{\mathbf{t}}^u \mathbf{t}^v\right\|} \tag{1.13}$$

where the tilde ($\sim$) over a vector indicates that its components are used for the skew-symmetric matrix used for a cross product [12]. To obtain the orthonormal referential associated to each contact point, the tangent vector $\mathbf{t}$ and the binormal vector $\mathbf{b}$ are

$$\mathbf{t} = \mathbf{t}^u / \left\|\mathbf{t}^u\right\|, \quad \mathbf{b} = \tilde{\mathbf{n}}\mathbf{t} \tag{1.14}$$

Note that in the calculation of the normal vector it assumed that there is no parametrization degeneration and, therefore, $\mathbf{t}^u$ and $\mathbf{t}^v$ are not parallel.

The parametrizations defined by Eqs. (1.1) and (1.4), for the spatial curve and surface respectively, do not ensure that these have constant velocity, i.e., that equal increases of a parameter in two different parts of the geometric shape lead to curve segments with different arc-length. Before the geometries can be used the parameters u, defining the curve, and u and v, defining the surface, need to be replaced by curve arc-length parameters L_u, for the curve, and L_u and L_v, for the surface, with respect to which the interpolating polynomial has a constant velocity. For instance, the parametric variable u^P of a curve, corresponding to a point P, located on the k^{th} polynomial segment is associated to a curve length L_k^P measured from the k^{th} segment origin, such that [43]

$$\int_0^{u^P} \sqrt{g_k^{u^T} g_k^u} du - L_k^P = 0 \tag{1.15}$$

In terms of its computer implementation, the non-linear Eq. (1.15) is solved in the program pre-processor, using Newton-Raphson method [12]. For the freeform surface, a similar procedure must be implemented for its re-parametrization.

For contact applications the evaluation of the positions of the points in the geometry and the corresponding normal and tangential vectors is often enough. However, when used to define kinematic constraints the derivatives of the normal and tangential vectors are also required. Therefore, the interpolation of curves and surfaces have minimum requirements in terms of the order of the interpolating polynomials that allow calculating all derivatives used in the formulation of the kinematic constraints [44].

1.2.2 Lookup Tables for Computational Efficiency

In a general computer implementation, it may be too costly to evaluate online the point positions, vectors and vector derivatives required by a particular problem. Take the case of a general contact problem of a multibody system in which there are multiple contact pairs between different surfaces, as in the case of rail-wheel contact for railway vehicles, or the case of a multibody system in which kinematic constraints are defined between curves and bodies, as in a roller coaster application [43]. Instead performing all calculations of the spatial geometry online it is computationally more efficient to use lookup tables (LuT) in which all quantities are pre-calculated as function of the curves and surfaces parameters and, at most, interpolated linearly [66].

After selecting any of the parametric descriptions of the spatial curve, the length parameter step ΔL_u adopted for the database construction is chosen, such a way that the any linear interpolation leads to an error, with respect to the exact value of any of the table contents, below a specified threshold [43]. The geometric parameters are organized in 37 columns as function of the length parameter L_u of the curve, as shown in Fig. 1.3.

Assume any freeform surface interpolation scheme for the surface and a re-parameterization with the arc-length parameter steps ΔL_u and ΔL_v adopted for the database construction. Also assume that the length parameter steps are selected such a way that the bi-linear interpolation leads to interpolation errors smaller then a specified threshold. The geometric parameters are organized in $1+\Delta L_v \times 12$ columns as function of the length parameter L_u of the curve, as shown in Fig. 1.4.

There are two clear problems with the LuT organized in the form described in Fig. 1.3 and in Fig. 1.4: The sequential access to the surface LuT is computationally inefficient when progressing along the arc-length parameter L_v, and for long curves,

	For constraints and contact				For kinematic constraints only							
L_u	$\mathbf{g}^T$	$\mathbf{t}^T$	$\mathbf{b}^T$	$\mathbf{n}^T$	$\frac{d\mathbf{g}^T}{dL_u}$	$\frac{d^2\mathbf{g}^T}{dL_u^2}$	$\frac{d\mathbf{t}^T}{dL_u}$	$\frac{d\mathbf{b}^T}{dL_u}$	$\frac{d\mathbf{n}^T}{dL_u}$	$\frac{d^2\mathbf{t}^T}{dL_u^2}$	$\frac{d^2\mathbf{b}^T}{dL_u^2}$	$\frac{d^2\mathbf{n}^T}{dL_u^2}$
0	…	…	…	…	…	…	…	…	…	…	…	…
ΔL_u	…	…	…	…	…	…	…	…	…	…	…	…
…	…	…	…	…	…	…	…	…	…	…	…	…
$n_u\Delta L_u$	…	…	…	…	…	…	…	…	…	…	…	…

Fig. 1.3 Structure of a look-up-table of a spatial curve geometry for application on the definition of path-following kinematic constraints or in contact

L_v	0				ΔL_u					$n_u\Delta L_u$			
L_u	$\mathbf{g}^T$	$\mathbf{t}^T$	$\mathbf{b}^T$	$\mathbf{n}^T$	$\mathbf{g}^T$	$\mathbf{t}^T$	$\mathbf{b}^T$	$\mathbf{n}^T$	…	$\mathbf{g}^T$	$\mathbf{t}^T$	$\mathbf{b}^T$	$\mathbf{n}^T$
0	…	…	…	…	…	…	…	…		…	…	…	…
ΔL_u	…	…	…	…	…	…	…	…		…	…	…	…
…	…	…	…	…	…	…	…	…		…	…	…	…
$n_u\Delta L_u$	…	…	…	…	…	…	…	…		…	…	…	…

Fig. 1.4 Structure of a look-up-table of a freeform surface geometry for application in contact

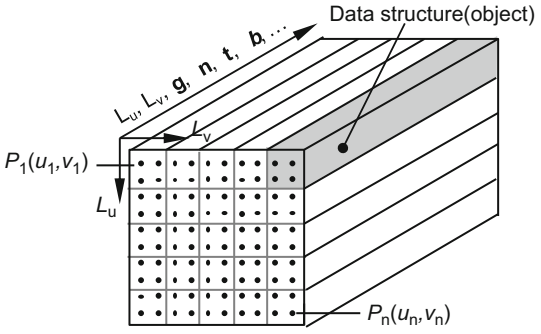

Fig. 1.5 Schematic representation of the lookup table of a surface

or large surfaces, with small arc-length steps the size of the table becomes too large to keep in memory. The first problem is easily addressed when using objects, or structures, in the computational implementation of the LuT, as implied in Fig. 1.5. Each element (i,j) of the structure, with the dimension of $n_u \times n_v$, contains the arc-length parameters L_u and L_v and vectors $\mathbf{g}$, with the point position in the surface reference frame, $\mathbf{t}$, $\mathbf{b}$ and $\mathbf{n}$. If the LuT is to be used in the definition of kinematic constraints, the parametric derivatives of the point position and vectors may also be necessary [66].

A bilinear interpolation of the twelve point coordinates and vector components is performed in each instant of simulation in order to evaluate all the relevant geometric information for the contact detection process [43, 66]. Note that the accuracy of the interpolation is solely dependent on the arc-length step of the table,

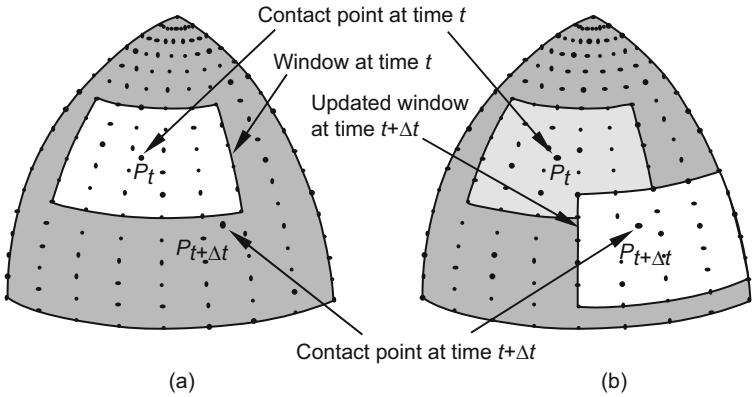

Fig. 1.6 Representation of an update of a storage window for: (**a**) Time step t; Time step $t+\Delta t$

being this chosen such a way that a pre-defined maximum interpolation error is never exceeded.

The partial reading of a surface file is suitable for contact point searching, in particular when the surface file is very large or when different rigid bodies share common geometric features. In these cases, the storage window must contain the contact zone, i.e., it should contain the records to which the candidate contact points belong. Figure 1.6a shows one eighth of a spherical surface, previously illustrated in Fig. 1.2b, with a storage window that includes the contact point at the instant of time t. If at the next instant of time, $t+\Delta t$, the contact point remains in a region close to the previous contact point, the storage window does not need to be updated. In contrast, when the next contact point approaches the border of the current window, the storage window has to be updated such that the contact point is centered in the new window, as in Fig. 1.6b.

The need for updating the storage window is checked in each contact calculation. This process is summarized by the following steps:

1. Locate contact record, i.e., the record that contains the initial guess (u_0,v_0);
2. Check if contact record belongs to storage window. If not, go to step (4);
3. Check if contact record is a border record. If not, go to step (7);
4. Locate storage window considering the contact record the center of the new storage window;
5. Store the index of the records of the new storage window, namely the first record and the border records;
6. Read and store the data of the records that belong to the new window;
7. Proceed with the contact computation.

The possibility to read partially the surface is useful in the cases where the contact point moves slightly and smoothly and, therefore, it remains in the vicinity of the previous contact point. Thus, the amount of memory used is significantly reduced and the contact detection process is more efficient.

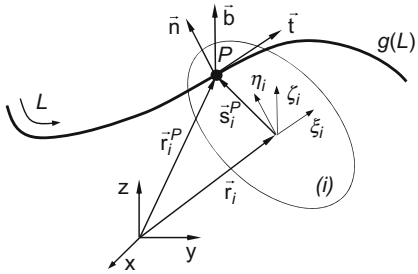

Fig. 1.7 Prescribed motion constraint, enforcing a body to follow a curve and its orientation to follow that of the curve moving frame

1.2.3 Kinematic Constraints with Spatial Curves

The definition of motion prescribed constraints along a spatial curve are used in cams, path-following joints or in roller coasters, among others. To define a kinematic joint in which the motion of a body is constrained to follow a spatial curve, consider a point P, located on a rigid body i constrained to follow a path, as in Fig. 1.7. The path is defined by a parametric curve $\mathbf{g}(L_u)$, in which is parameter L_u represents the length travelled by the point along the curve from the origin to its current location. The constraint equations that enforce point P to follow the reference path $\mathbf{g}(L_u)$ are written as [43]:

$$\mathbf{\Phi}^{(pmc,3)} = \mathbf{0} \quad \equiv \quad \mathbf{r}_i^P - \mathbf{g}\,(L_u) = \mathbf{0} \tag{1.16}$$

where $\mathbf{r}_i^P$ is the position vector associated to point P, depicted in Fig. 1.7.

The prescribed motion constraint also ensures that the spatial orientation of body i remains unchanged with respect to the moving Frenet frame $(\mathbf{t},\mathbf{n},\mathbf{b})$ associated to the curve. Consider a rigid body i where $(\mathbf{u}_\xi,\ \mathbf{u}_\eta,\ \mathbf{u}_\zeta)_i$ represent the unit vectors associated to the axes of $(\xi,\eta,\zeta)_i$ defined in the body frame. Consider also that the Frenet frame of the general parametric curve $\mathbf{g}(L)$ is defined by the principal unit vectors $(\mathbf{t},\ \mathbf{n},\ \mathbf{b})_L$, as depicted in Fig. 1.7. The relative orientation between the body vectors $(\mathbf{u}_\xi,\mathbf{u}_\eta,\mathbf{u}_\zeta)_i$ and the curve local frame $(\mathbf{t},\ \mathbf{n},\ \mathbf{b})_L$ must be such that [43]:

$$\mathbf{\Phi}^{(lfac,3)} = \begin{Bmatrix} \mathbf{n}^T \mathbf{A}_i \mathbf{u}_\xi \\ \mathbf{b}^T \mathbf{A}_i \mathbf{u}_\xi \\ \mathbf{n}^T \mathbf{A}_i \mathbf{u}_\eta \end{Bmatrix} - \begin{Bmatrix} a \\ b \\ c \end{Bmatrix} = 0 \tag{1.17}$$

where $\{a \quad b \quad c\}^T = \text{diag}\left[\left(\mathbf{A}_L^{\mathbf{0}}\right)^T \mathbf{A}_i^{\mathbf{0}}\right]$ are constants calculated at the initial time of the analysis by using Eq. (1.17) with the initial conditions. The contribution of the prescribed motion constraint to the constraint acceleration is written as

$$\begin{bmatrix} \mathbf{\Phi}_{\mathbf{q}}^{(pmc,3)} \\ \mathbf{\Phi}_{\mathbf{q}}^{(lfac,3)} \end{bmatrix} \ddot{\mathbf{q}} = \begin{bmatrix} \boldsymbol{\gamma}^{(pmc,3)\#} \\ \boldsymbol{\gamma}^{(lfac,3)\#} \end{bmatrix} \tag{1.18}$$

where the Jacobian matrix associated to each part of the kinematic constraint is

$$\boldsymbol{\Phi}_{\mathbf{q}}^{(pmc,3)} = \left[\, \mathbf{I} \; -\tilde{\mathbf{s}}_i^R \mathbf{A}_i \; -\boldsymbol{d}\mathbf{g}/dL \,\right] \tag{1.19}$$

$$\boldsymbol{\Phi}_{\mathbf{q}}^{(lfac,3)} = \begin{bmatrix} \mathbf{0}^T & - & \mathbf{n}^T \mathbf{A}_i \tilde{\mathbf{u}}_\xi & (\boldsymbol{d}\mathbf{n}/dL)^{\boldsymbol{T}} \mathbf{A}_i \mathbf{u}_\xi \\ \mathbf{0}^T & - & \mathbf{b}^T \mathbf{A}_i \tilde{\mathbf{u}}_\xi & (\boldsymbol{d}\mathbf{b}/dL)^{\boldsymbol{T}} \mathbf{A}_i \mathbf{u}_\xi \\ \mathbf{0}^T & - & \mathbf{n}^T \mathbf{A}_i \tilde{\mathbf{u}}_\zeta & (\boldsymbol{d}\mathbf{n}/dL)^{\boldsymbol{T}} \mathbf{A}_i \mathbf{u}_\zeta \end{bmatrix} \tag{1.20}$$

and the contribution of each part of the kinematic constraint to the right hand side of the acceleration equations is

$$\boldsymbol{\gamma}^{(pmc,3)\#} = -\tilde{\boldsymbol{\omega}}_i \, \dot{\mathbf{s}}_i^R + \frac{d^2\mathbf{g}}{\boldsymbol{dL}^2} \, \dot{\boldsymbol{L}}^2 \tag{1.21}$$

$$\boldsymbol{\gamma}^{(lfac,3)\#} = -\left\{ \begin{array}{l} \left[2\,\dot{L}(d\mathbf{n}/d\mathrm{L})^T \mathbf{A}_i \tilde{\boldsymbol{\omega}}'_i + \mathbf{n}^{\boldsymbol{T}} \mathbf{A}_i \tilde{\boldsymbol{\omega}}'_i \tilde{\boldsymbol{\omega}}'_i + \dot{L}^2 \left(d^2\mathbf{n}/dL^2\right)^{\boldsymbol{T}} \mathbf{A}_i \right] \mathbf{u}_\xi \\ \left[2\,\dot{L}(d\mathbf{b}/\boldsymbol{d}L)^{\boldsymbol{T}} \mathbf{A}_i \tilde{\boldsymbol{\omega}}'_i + \mathbf{b}^{\boldsymbol{T}} \mathbf{A}_{\boldsymbol{i}} \tilde{\boldsymbol{\omega}}'_{\boldsymbol{i}} \tilde{\boldsymbol{\omega}}'_{\boldsymbol{i}} + \dot{L}^2 \left(d^2\mathbf{b}/\boldsymbol{d}L^2\right)^{\boldsymbol{T}} \mathbf{A}_i \right] \mathbf{u}_\xi \\ \left[2\,\dot{L}(\boldsymbol{d}\mathbf{n}/\boldsymbol{d}L)^T \mathbf{A}_i \tilde{\boldsymbol{\omega}}'_{\boldsymbol{i}} + \mathbf{n}^{\boldsymbol{T}} \mathbf{A}_{\boldsymbol{i}} \tilde{\boldsymbol{\omega}}'_{\boldsymbol{i}} \tilde{\boldsymbol{\omega}}'_{\boldsymbol{i}} + \dot{L}^2 \left(d^2\mathbf{n}/dL^2\right)^{\boldsymbol{T}} \mathbf{A}_{\boldsymbol{i}} \right] \mathbf{u}_\zeta \end{array} \right\} \tag{1.22}$$

The minimum requirements for the degree of the interpolating polynomials that can be used in the formulation of the prescribed motion constraint is associated to the order of the derivatives used in Eqs. (1.16, 1.17, 1.18, 1.19, 1.20, 1.21 and 1.22). The right hand side vector in Eq. (1.21) involves $d^2\mathbf{n}/dL^2$ being $\mathbf{n} = \mathbf{k}/\|\mathbf{k}\|$ given by Eq. (1.9) and $\mathbf{k} = \mathbf{g}^{uu} - (\mathbf{g}^{uuT}\mathbf{g}^u)\mathbf{g}^u/\|\,\mathbf{g}^u\|^2$ by Eq. (1.10). Therefore, it is required that the fourth derivative of the interpolating polynomial is used, being a quintic polynomial the lowest odd degree polynomials to be used to formulate accurately the prescribed motion constraint [44].

1.2.4 Application in a Roller Coaster Dynamics Study

Roller coasters are, apparently, relatively simple mechanical systems when compared to modern railways or cars, but are a perfect examples for using spatial curve geometries. Since most roller coasters represent unique designs, extensive testing of real world prototypes is not possible from an economical point of view, being computational tools of important for virtual testing before the construction of the roller coaster track. The geometric description of the curve for a roller coaster track starts with the definition of a moving referential, being the track used in this application depicted by the sweep of the normal and binormal vectors shown in Fig. 1.8. The individual geometry of each rail of the roller coaster track is obtained from the definition of the centerline and track torsion using the moving frames

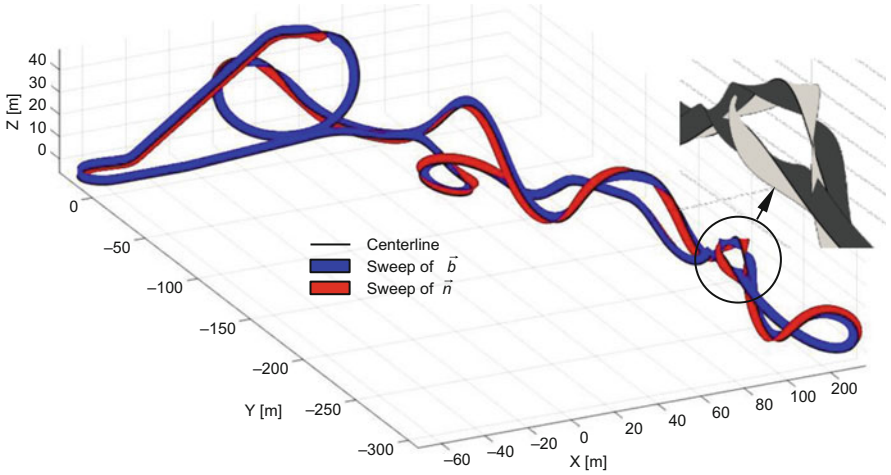

Fig. 1.8 Roller coaster track with the identification of the sweeps of the normal and binormal vectors of the moving frame, highlighting a corkscrew segment of the track

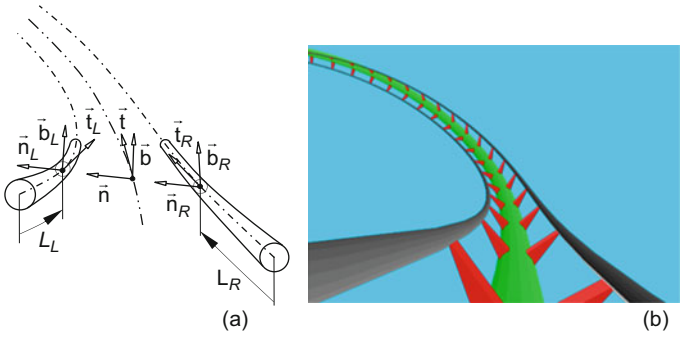

Fig. 1.9 Spatial description of the roller coaster rails: (**a**) Frenet and rails moving frames: (**b**) Geometry of the rails for a roller coaster

shown in Fig. 1.9. Note that, in the definition of the moving referential there are singularities in the straight track segments, as discussed by Tandl and Kecskemethy [45, 46], that are handled by enforcing the normal vector to be parallel to the XY plane. Furthermore, due to the long track length, LuT are used in the implementation of the path following kinematic constraints.

A model of a roller coaster vehicle and biomechanical multibody model are developed, and described in the work by Viegas et al. [67], being its dynamics analyzed with the objective of studying the occupant exposure to injurious conditions. The motion resulting from the simulation of the roller coaster is depicted in Fig. 1.10 with selected frames of the vehicle and passenger motion.

The track torsion is the rotation of the track tangent plane, about the tangent vector, with respect to the plane defined by the tangent and normal vectors of the

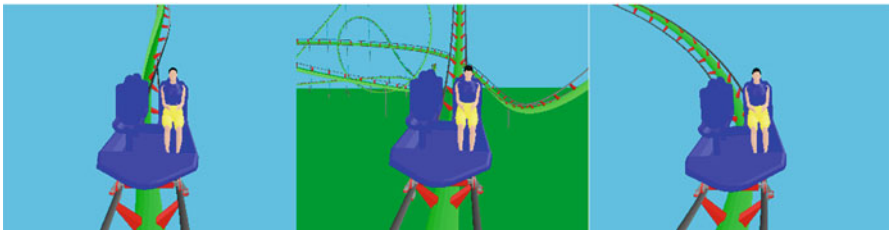

Fig. 1.10 Selected frames from the motion of a roller coaster vehicle with an occupant

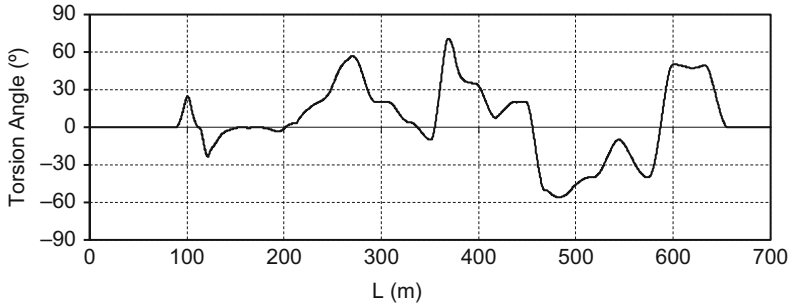

Fig. 1.11 Track torsion along its complete length

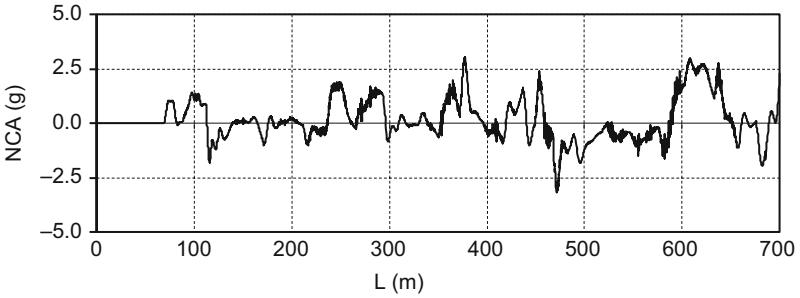

Fig. 1.12 Non-compensated acceleration of a passenger seating in the front left seat

Frenet frame associated to the track centerline, being its evolution for the roller coaster track considered here shown in Fig. 1.11. The design of the evolution of the torsion is used not only for some of the thrills of a roller coaster ride but also to allow controlling the lateral accelerations experienced by roller coaster passengers.

Among other results of interest from the dynamic analysis of the roller coaster, those associated to the rider safety are of importance, being the non-compensated acceleration, directly associated to the lateral accelerations experienced by the rider, shown in Fig. 1.12, one of the representative quantities.

The analysis of the non-compensated acceleration, and other biomechanical injury criteria, allows the designer to reshape the segments to avoid the passenger

exposure to be close to any injurious condition. Another form of using the passenger data is in the redesign of the track to obtain the thrills and emotions desired by roller coaster users.

1.3 Contact Mechanics in Multibody Systems

Contact problems present some of the most important challenges of the correct and efficient definition of complex spatial geometries in multibody dynamics. Contact mechanics involves the solution of two basic sub-problems: the contact detection and the contact force modelling. In this work the contact identification problem is analyzed and continuous contact models, based on Hertzian and non-Hertzian elastic contact are considered. Nonsmooth mechanics approaches are not considered here, although they offer good alternatives to handle contact mechanics [51, 57–60, 68]. The numerical issues associated with the contact-impact mechanics are also overviewed in the process, receiving the implications of the contact force modelling on time integration attention [69, 70].

1.3.1 Search of Contact Between Two Generic Surfaces

Let it be assumed that a body in motion approaches another. These bodies can be described as generic surfaces, which can be represented as shown in Fig. 1.13. At any given instant, there are always two points which are closest to each other and where contact is more likely to occur. The search for contact between the two surfaces requires the identification of two parameters of each surface, associated to the location of the points that are either in contact or in closer proximity. This is illustrated in Fig. 1.13a, in which the points in closer proximity are depicted as P and Q, each belonging to a generic surface on body i and j, respectively. The surfaces are defined in the referentials $(\xi\eta\zeta)_i$ and $(\xi\eta\zeta)_j$ fixed to the centers of mass of bodies i and j, respectively. Vector $\mathbf{d}$ represents the distance between them, given by $\mathbf{d} = \mathbf{r}_P - \mathbf{r}_Q$.

Still with reference to Fig. 1.13, on point P in body i the vector normal to the surface is $\mathbf{n}_P$ while $\mathbf{t}_P$ and $\mathbf{b}_P$ are the tangent and binormal vectors to the surface, respectively, forming an orthogonal basis. The same applies to $\mathbf{n}_Q$, $\mathbf{t}_Q$ and $\mathbf{b}_Q$, which are the vectors on point Q. The relation between the components of the different vectors defined in each body and the parameters used to define the surface depends on the specific geometry of the contacting surface. The conditions for minimal distance between the two surfaces are that points P and Q are generically described by [71],

$$\begin{cases} \mathbf{d}^T\ \mathbf{t}_Q = 0 \\ \mathbf{d}^T\ \mathbf{b}_Q = 0 \end{cases} \quad ; \quad \begin{cases} \mathbf{n}_Q^T\ \mathbf{t}_P = 0 \\ \mathbf{d}^T\ \mathbf{b}_P = 0 \end{cases} \tag{1.23}$$

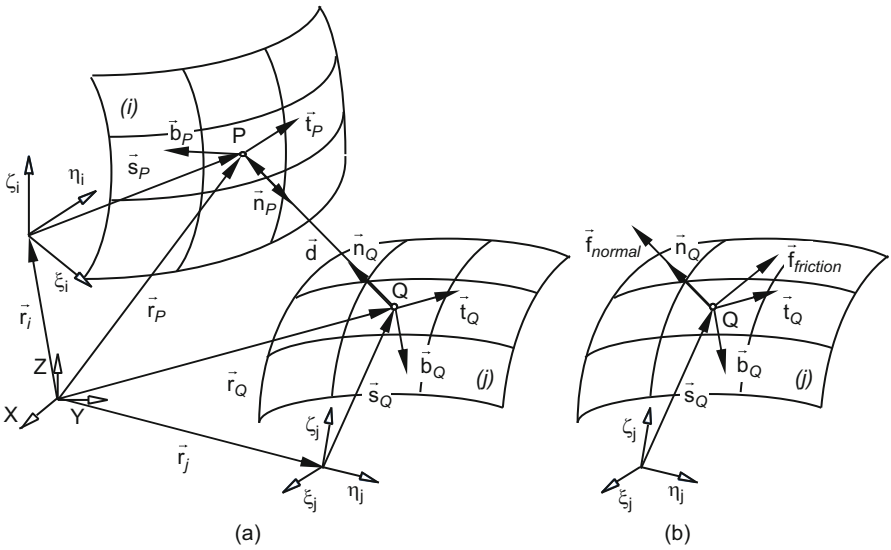

Fig. 1.13 Contact points candidates in two parametric surfaces. Point P belongs to a surface on body i and point Q to a surface on body j: (**a**) Contact detection; (**b**) Contact forces in body i

which means that not only the normal to each surface must be collinear with the vector that connects the two points in closer proximity but also perpendicular to the tangent and binormal vectors on each point. Effective contact occurs if, besides the fulfilment of Eq. (1.23), penetration also exists, which is expressed by,

$$\delta = \mathbf{d}^T \ \mathbf{n}_Q \leq 0 \tag{1.24}$$

otherwise, the points are in close proximity, but not in contact.

1.3.2 Simple Continuous Contact Force Models

When contact between two surfaces exists both normal and friction forces develop, as highlighted in Fig. 1.13b. Depending on the application, the constitutive equations for the frictions forces may be simple or very complex. Road vehicle dynamics, in which the tire to road contact forces are described by elaborate tire models [72, 73], railway dynamics, in which the wheel to rail contact lead to friction forces requiring a rather complex interaction [71, 74], or even in lubricated rotating machinery, in which the tribological tangential forces are associated to lubrication modes and specific lubrication force models [75], present examples of systems for which the tangential contact forces calculation require complex constitutive laws.

However, for many applications of multibody systems simpler interaction force models are devised, mostly based on Hertzian contact conditions.

The modified Kelvin-Voigt's visco-elastic contact model [47, 50] is a simple continuous normal contact force model that relates the interference between two surfaces with a normal reaction force, formulated as,

$$f_{normal} = K\ \delta \begin{cases} c_e & \dot{\delta} \leq 0 \\ \left[c_e + (1 - c_e)\left(3r^2 - 2r^3\right)\right] & 0 < \dot{\delta} < v_0 \\ 1 & \dot{\delta} \geq v_0 \end{cases} \tag{1.25}$$

with the ratio between the penetration velocity and the penetration velocity tolerance being $r = \dot{\delta}/v_0$, a penalty stiffness K and a coefficient of restitution c_e. The penetration velocity tolerance, pre-defined by the user as being $v_0 = 0.1$ m/s is often used. Note that the modified Kelvin-Voigt normal contact force model includes the penetration velocity tolerance to smooth the discontinuity in the contact force in the transition between compression and restitution but also includes an energy dissipation term during the restitution contact phase.

The normal contact force model proposed by Lankarani and Nikravesh [76] is based on the assumption for Hertzian contact and also includes a dissipative term based on the Hunt-Crossley model [77]. This normal force contact model is suitable for low impact velocities in which local plasticity effects do not develop or are negligible,

$$f_{normal} = K\ \delta^n \left[1 + \frac{3\left(1 - c_e^2\right)}{4} \frac{\dot{\delta}}{\dot{\delta}^{(-)}}\right] \tag{1.26}$$

where δ is evaluated using Eq. (1.24), and includes the relative stiffness of the contacting surfaces K, the pseudo-penetration exponent n and the restitution coefficient c_e dependent on the geometry and material of the contacting surfaces. $\dot{\delta}$ is the velocity of indentation and $\dot{\delta}^{(-)}$ is the velocity of indentation at the initial instant of contact. Note that ratio $\delta/\dot{\delta}^{(-)}$ leads to numerical problems for very small velocities of indentation at the start of contact, i.e., when $\dot{\delta}^{(-)} \approx 0$. In the computational implementation of the Lankarani and Nikravesh model, or any other that has the dissipative part written in the same form, the ratio $\delta/\dot{\delta}^{(-)} = 1$ when the penetration velocity $\dot{\delta}$ exceeds $\dot{\delta}^{(-)}$ or when $\dot{\delta}^{(-)} \approx 0$.

The contact between two surfaces not only generates normal forces but also friction forces, if the relative tangential velocity between the surfaces is not null. The Amontons-Coulomb friction model is not only the most common form of describing the friction forces but also the basis for many other models. Here, this friction force model is modified to include a regularization term to prevent numerical problems during integration of the system equations of motion, being [47].

$$f_{friction} = -c_f c_d f_{normal} \dot{\delta} / \left|\dot{\delta}\right| \tag{1.27}$$

where c_f is the dynamic friction coefficient, c_d a numerical regularization factor and $\dot{\delta}$ is the relative angular velocity of the bodies connected by the joint. The regularization factor proposed by Threfal is the exponential function $c_d = 1 - \exp\left(-3\dot{\delta}/v_1\right)$ while Ambrósio [78] proposes a ramp function defined as $c_d = 0$ for $\dot{\delta} \leq v_0$, $c_d = \left(\dot{\delta} - v_0\right) / \left(v_1 - v_0\right)$ for $v_1 \leq \dot{\delta} \leq v_0$ and $c_d = 1$ otherwise. Therefore, the input parameters for these models are the dynamic friction coefficients c_f, the threshold velocities v_0 and v_1 and the joint friction tuning normal force f_n.

In a wide number of contact problems, the transition between static and dynamic friction plays an important role. The Stribeck effect aims at representing numerically such transition with continuous and smooth numerical description. There are several friction models, which include the Stribeck effect to represent static friction, proposed [79]. Among these, the Bengisu and Akay model, with good numerical characteristics to be used in contact problems, is defined by [80]

$$n_{friction} = -f_{normal}\dot{\delta}/\left|\dot{\delta}\right| \begin{cases} \frac{c_s}{v_0^2}\left(\left|\dot{\delta}\right| - v_0\right)^2 + c_s & \left|\dot{\delta}\right| \leq v_0 \\ c_f + \left(c_f - c_s\right) e^{-\xi\left(\left|\dot{\delta}\right| - v_0\right)} & \left|\dot{\delta}\right| > v_0 \end{cases} \tag{1.28}$$

where v_0 is the Stribeck velocity, c_s is the static friction coefficient and ξ is the curve shape factor, typically in the order of to 50 s/rad.

The use of friction models that include the Stribeck effect, such as the Bengisu and Akay model, have the advantage of representing the transition from static to dynamic friction better than those described by Eq. (1.27). Other alternative friction models, are designed to better capture the pre-sliding displacement and the frictional lag, being designated as dynamic friction models [79]. Among these the Gonthier friction model, which is an evolution of the LuGre friction model, shows good numerical properties being suitable for applications in which the stick-slip transitions play important roles in the system dynamics. Due to their complexity they are not overseen in this work being the interested reader referred to the work by Marques et al. [79].

1.3.3 Numerical Aspects of the Contact Analysis

One of the critical aspects in the dynamic simulation of the multibody systems with collisions is the detection of the precise instant of contact. The contact duration and the penetration cannot be predicted from the pre-impact conditions due to the influence of the kinematic constraints imposed in the bodies on the overall system motion. Thus, before the first impact, the bodies can freely move relative to each other and, in this phase, the step size of the integration algorithm may become relatively large. Therefore, if the numerical integration is not handled properly, the first impact between the colliding bodies is often made with a high penetration depth, and, hence, the calculated contact forces becomes artificially large.

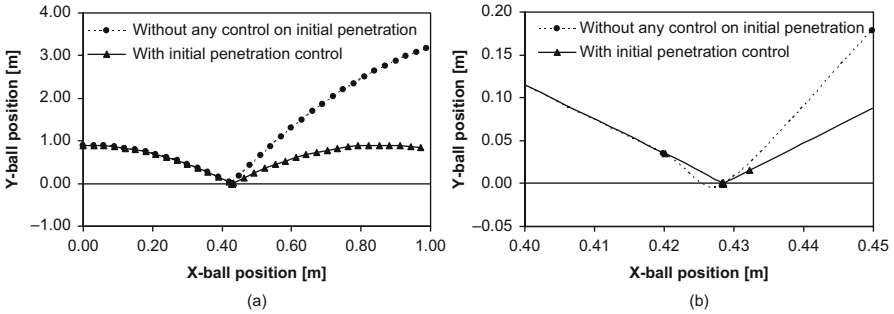

Fig. 1.14 (**a**) Trajectory of a falling ball obtained with integration algorithms with and without initial penetration control; (**b**) Detailed view in the vicinity of contact

The importance of the initial penetration control, in the framework of the integration of the equations of motion, is better discussed using a simple example [69]. Take the case of the falling ball illustrated in Fig. 1.14, animated by an initial horizontal velocity and acted upon by gravity forces only. The motion of the ball is such that during its falling trajectory it strikes the ground. The penetration of the ball in the ground, in the integration time step, for which contact is first detected, is,

$$\delta^{(-)} = (h - R) - y_b \tag{1.29}$$

where y_b is the y coordinate of the ball center of mass. The superscript $(-)$ on δ means that it is the penetration when contact is first detected. Note that $\delta^{(-)}$ must be a positive value for contact. Therefore, by monitoring the sign of the penetration at every time step $t+\Delta t$ the start can be identified from,

$$\delta^{(-)}(\mathbf{q}, t)\, \delta^{(-)}(\mathbf{q}, t + \Delta t) \leq 0 \tag{1.30}$$

When Eq. (1.30) is fulfilled the start of contact occurs at $t+\Delta t$. The integration of the equations of motion of the system can proceed with no numerical problem if the penetration first detected is close to zero, or at least below a pre-defined threshold, i.e., if $\delta^{(-)}(\mathbf{q}, t + \Delta t) \leq \delta_{max}$. Because this is not always the case, strategies to limit the time step in the vicinity of contact must be implemented when solving contact problems [69].

Define as δ^- the distance between the two surfaces in the time step t^- that precedes the time step t^+, at which penetration δ^+ is first detected. In between these time steps, say at t^c, the penetration $\delta^c = 0$ exists. Assuming constant velocity for the multibody system in the vicinity of contact, the time at which contact starts can be calculated by,

$$t^c = t^- + \frac{\delta^-}{\delta^+ - \delta^-} \Delta t \tag{1.31}$$

Consequently, the ideal situation, during the integration of the multibody equations of motion, would be that a time step in the vicinity of contact to be

$$\Delta t^{ideal} = t^c - t^- + \varepsilon \tag{1.32}$$

where ε is a very small number to effectively ensure that $\delta_{max} > \delta^c > 0$. Several procedures are suggested to ensure that $\delta^+ < \delta_{max}$, can be implemented, depending on the access that exists to the numerical integrator. Several strategies are proposed by Flores et al. [69] to handle the numerics associated to the regularization of the time integration of the multibody equations of motion, being the interested reader referred to their work.

1.3.4 Selected Applications

The applications explored here for contact between bodies with a prescribed geometry are intended to identify and propose solutions for pitfalls in the contact detection and to present realistic application cases with rather complex contact mechanics. The solution of the contact between simple surfaces, circles in a planar contact case and cylinders in a spatial case, explore the pitfalls on the contact detection and propose measures to avoid them. The wheel-rail contact problem, associated to railway dynamics, presents a more complex, and realistic, contact problem for which the procedures outlined in this work are of fundamental importance.

1.3.4.1 Circle-to-Circle and Cylinder-to-Cylinder Contact Detection

The contact identification problem of two circles in a two-dimensional space is used here not only to test the contact detection procedures presented but also to identify pitfalls of the numerical methods involved. According to Fig. 1.15a, the local position of the potential contact points in the surfaces are $\mathbf{s}_i'^P = R_j\{\cos\ \varphi_j \quad \sin\ \varphi_j\}^T$ and $\mathbf{s}_i'^Q = R_i\{\cos\ \varphi_i \quad \sin\ \varphi_i\}^T$, while the normal and tangential vectors associated to the surfaces on those points are $\mathbf{n}_P = \mathbf{A}_j\{\cos\ \varphi_j\ \sin\ \varphi_j\}^T$, $\mathbf{t}_P = \mathbf{A}_j\{\sin\ \varphi_j\ -\cos\ \varphi_j\}^T$, $\mathbf{n}_Q = \mathbf{A}_i\{\cos\ \varphi_i\ \sin\ \varphi_i\}^T$ and $\mathbf{t}_Q = \mathbf{A}_i\{\sin\ \varphi_i\ -\cos\ \varphi_i\}^T$, being R_i and R_j the circle radios. The conditions for minimal distance are defined, in this planar case, as:

$$\begin{cases} \mathbf{n}_j^T \mathbf{t}_i = 0 \\ \mathbf{d}^T \mathbf{t}_i = 0 \end{cases} \tag{1.33}$$

which is solved using any solver for systems of nonlinear equations, such as the Newton-Raphson method, optimization based procedures or other suitable approach [81].

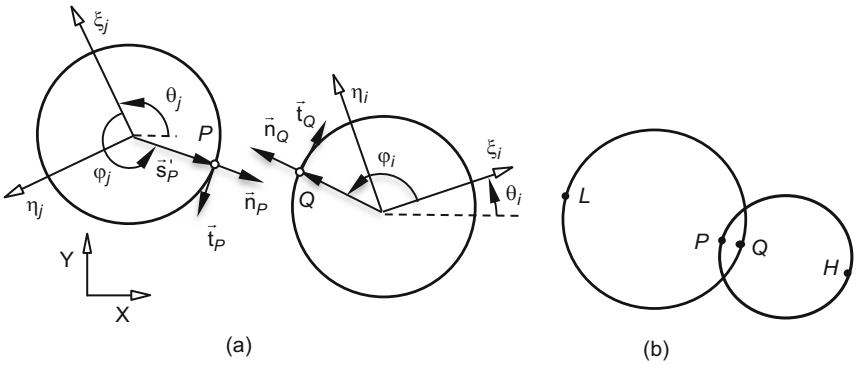

Fig. 1.15 Geometric relations describing the positions of points P and Q in two circles; (**a**) Geometric definitions for the contact problem; (**b**) Potential contact points to form the contact pairs

Table 1.1 Results from contact point detection for two random circles

Matlab method	Success rate (%)	Computer time (s)
`Newton-Raphson`	66.7	0.10
`fsolve`	100	0.15
`fmincon`	100	0.37

This system of nonlinear equations has four solutions for potential contact points, depicted as the pairs of points PQ, HP, QL and LH. Although, by visual inspection of Fig. 1.15b, it is clear that PQ represent the contact pair there is no reason for the solution of the system of nonlinear equations converge for this pair and not to any of the others. To minimize the problem, a discrete method for finding a close guess to the solution is necessary so that the solver is guided to the solution closer to the guess. However, there is no assurance that another solution is not chosen instead.

To test the different methods to solve the nonlinear system of equations 100 pairs of circles are generated in random positions and orientations. With a Matlab® code in which the functions `NewtonRaphson`, `fsolve` and `fmincon` are used and the initial guess for the location of each pair of points in closest proximity are offered as the first guess for the solution to obtain a solution. By visual inspection of each of the solution found, the result is deemed successful or not. Table 1.1 presents the success rate of each of the methods tested as well as the computer time required to solve the 100 problems with each method tested.

This analysis clearly shows that Newton-Raphson is not always capable of finding the correct result in a reliable way, being the wrong solution always associated with contact pairs that exhibit a very large interference. Since in most, if not all, contact problems using rigid bodies the indentations are very small a limitation on the maximum indentation of 1% of the largest circle radius is set in the random generation of the 100 circle pairs. It is observed that for this new population the Newton-Raphson method has a success rate of 100% in finding the correct contact pair.

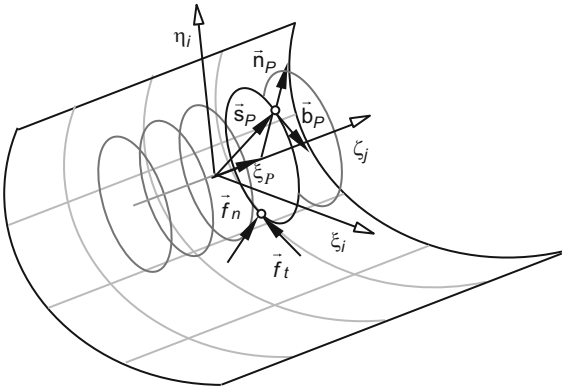

Fig. 1.16 Slice method applied to a cylindrical roller

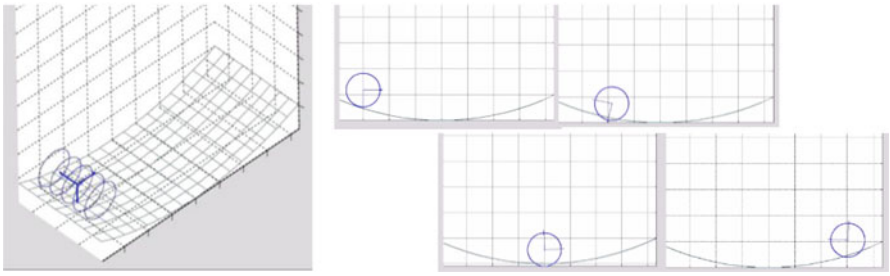

Fig. 1.17 3D view of the starting point for a roller on an internal cylindrical surface and its motion observed in a side view of the roller and cylindrical surfaces

An approach to model contact problems with spatial surfaces of revolution is the strip method, in which a revolution surface is discretized by a finite number of circles. Now, the contact of each individual circle with a surface, as shown in Fig. 1.16, is solved independently. In this form, the line contact associated to the contact pairs is discretized in a series of point contacts. This approach is used in roller bearing dynamics for the contact between the rollers and the raceways and cage [82] and in railway dynamics for cases in which the wheel profile leads to conformal wheel-rail contact [83].

The dynamics of the contact of the roller, using the slice discretization, on a cylindrical surface is computed for a period of time that allows the roller to travel for the complete arc-length of the cylinder, as shown in Fig. 1.17. The Kelvin-Voigt normal contact force model, described by Eq. 1.25, and the Amontons-Coulomb friction force model with Threfal smoothing, described by Eq. (1.27), are used in the contact.

A large number of initial conditions and material properties are simulated, each one of them using `Newton-Raphson, fsolve` and `fmincon` methods. It is observed that all methods used are successful in finding the correct solution of all contacts involved in the dynamics of the test case. However the computational

time required by each method is quite different, being `Newton-Raphson` always faster, `fsolve` about 1.5 times slower and `fmincon` about 4 times slower. The implementation of the Newton-Raphson method is more demanding than the other methods, as it requires that the Jacobian matrices for each contact pair are available. When dealing with several thousand of potential contact pairs in each time the equations of motion of the multibody system are solved, which may take place more than once per time step, as in the case of the dynamic analysis of roller bearings, computational efficiency becomes of major importance.

1.3.4.2 Wheel-Rail Interaction in Railway Dynamics

Railway dynamics involves, in general, the solution of the wheel-rail contact problem, which poses interesting challenges in terms of the contact detection but also on the modelling of the contact forces. From the point of view of the contact detection, the surface of revolution of the wheel may be convex or non-convex depending on its wear. The case presented here to illustrate the close relation between the contact problem and the geometrical description of the contact surfaces involves the operation of a light rail vehicle in an existing railway track.

The light rail vehicle, shown in Fig. 1.18, is composed by a carbody, for passengers, supported by two bogies. One bogie is powered by a diesel engine, the motor bogie, while the other one, the trailer bogie, is free. Each bogie is composed by a bogie frame, two wheelsets and four axleboxes, which include a primary suspensions. The carbody and bogie frames are connected by a secondary suspensions. Details of the railway vehicle multibody model can be found in the work by Magalhães et al. [84].

The vehicle operation is studied for a real railway track for which both for the horizontal nominal geometry, defined during the project, and for the current geometry, measured experimentally, are described in Fig. 1.19. Besides the curvature of track, as function of the track length, also the cant, the vertical profile and the track irregularities, all function of the track arc-length, are available and used for the study.

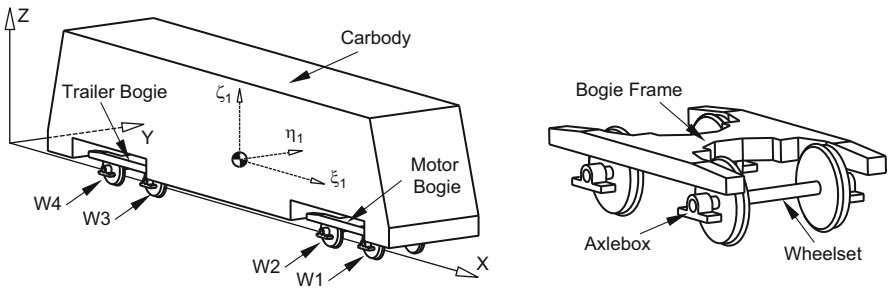

Fig. 1.18 Light Rail Vehicle multibody model with a more detailed bogie and wheelsets assembly

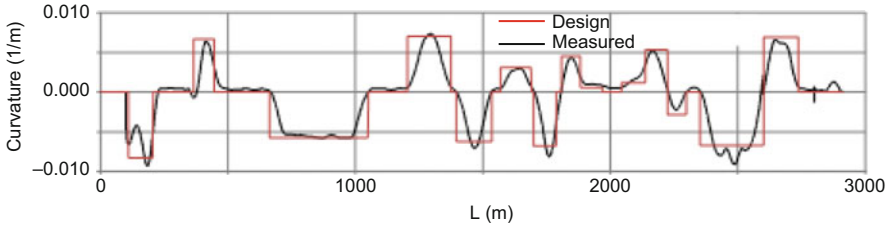

Fig. 1.19 Track curvature as function of the track arc-length for the measured and nominal data

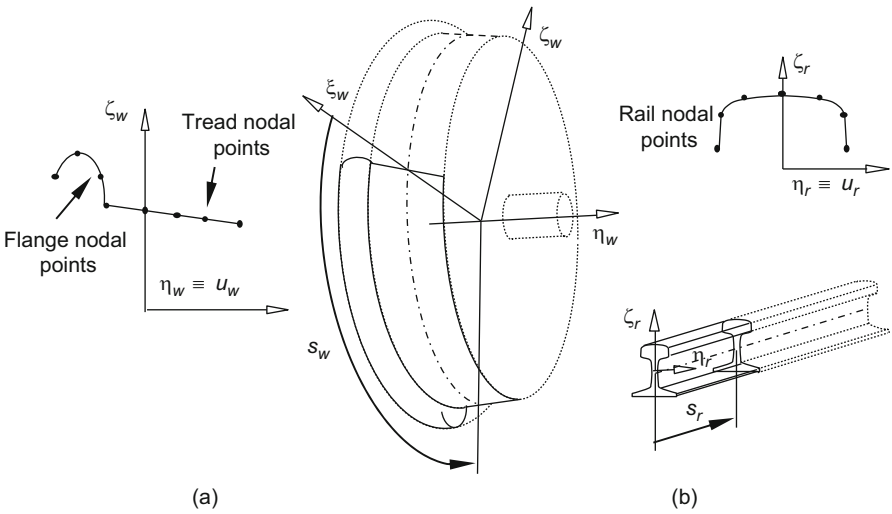

Fig. 1.20 Geometry of the bodies; (**a**) Wheel obtained as a surface of revolution of the wheel profile; (**b**) Rail surface obtained by sweeping the rail profile along the rail centerline

The surfaces of the rails, deemed as left and right rails, and the wheels, eight in each vehicle, are shown in Fig. 1.20 as sweep surfaces and surfaces of revolution, respectively. In the case of the wheel, there are, in fact, two surfaces of revolution, one for the tread and another for the flange. Therefore, the wheel rail contact between geometries with nominal configurations, i.e., geometries that are not worn, involves the solution of two independent problems per wheel-rail pairs: flange-to rail- and tread-to-rail contact [71].

Each one of the contact problems for each one of the railway vehicle wheels is solved using Eq. (1.23), leading to the identification of the contact points or those of closer proximity, as pictured in Fig. 1.21. This means that for each vehicle, equipped with eight wheels, sixteen contact problems need to be solved each time the equations of motion of the multibody system are solved. When contact is detected in each one of the contact pairs a normal contact force is evaluated using a contact model such as those described by Eqs. (1.25) or (1.26) and the creep, or tangential, forces are computed with an appropriate model, such as those proposed by Kalker [74], Polach [85], Chollet [86], Berg [87], Bruni [88], or similar.

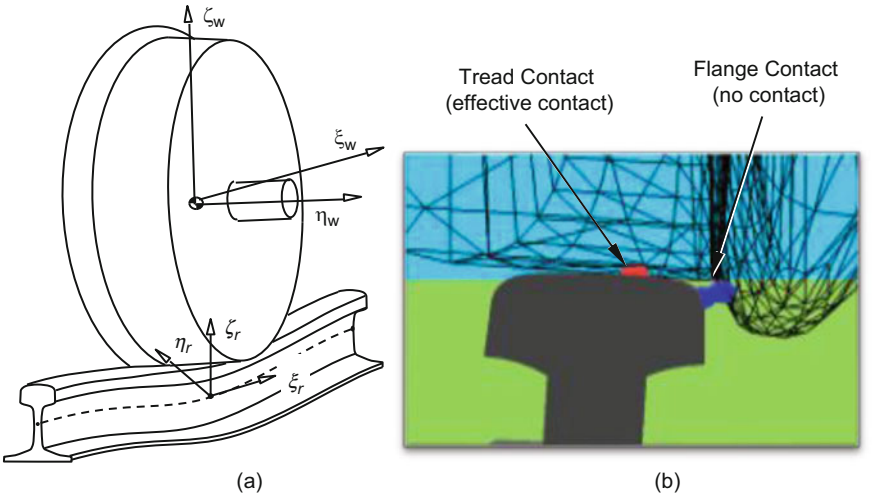

Fig. 1.21 Contact between wheel and rail; (**a**) Perspective view of the wheel-rail; (**b**) Identification of the independent treat-rail and flange rail contacts, where only the first is in effective contact

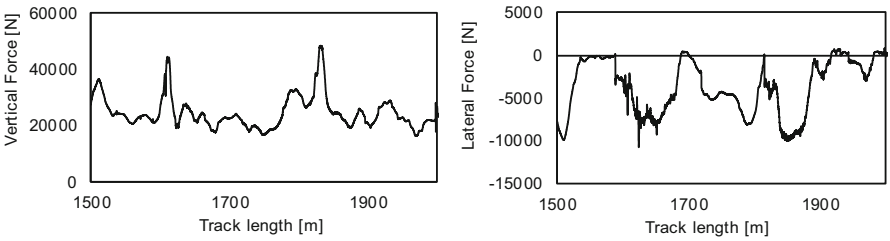

Fig. 1.22 Evolution of the wheel-rail contact forces along a section of the railway track

The rail-wheel contact force experienced by the vehicle wheels, for the scenario envisaged in this work, in which the vehicle is operating at a speed of 50 km/h, are illustrated by the normal and lateral, creep, forces shown in Fig. 1.22. It is noticeable the relation between the evolution of the lateral forces and the curves of the track.

The solution of the contact problem with non-worn wheels can be done online, as the work by Pombo et al. demonstrates [71]. However, it is also been demonstrated by some authors that computational efficiency is obtained from using LuT to identify the contact forces that develop in each contact pair [89]. In the case of worn, but still functional, wheel profile a conformal contact with the rail, for which the Hertzian contact force models do not apply, needs to be formulated. In this case, the wheel-rail contact is not only in the vicinity of a point but, eventually, in a larger region, being modelled as a multiple contact point problem. In these contact conditions the use of LuT to obtain the contact forces and the location of the equivalent contact points is unreplaceable, at least currently.

1.4 Perfect Kinematic Joints Versus Clearance Contact Joints

In a wide number of practical applications in multibody dynamics the kinematic joints are not perfect, exhibiting clearances and including elastomers to accommodate for misalignments and to damp vibrations. The inexistence of such features would not only impair the durability of the system but also prevent it from functioning properly [90–92]. The way of handling imperfect joints in multibody models is, instead of enforcing kinematic constraints between rigid bodies, by associating the relative displacements and rotations between the connected bodies to contact forces, i.e., by penalizing the relative displacements using appropriate constitutive relations due to contact, as for the clearance joints, or due to local elastic deformations, as for bushing joints. An overview of the general formulation proposed by Ambrosio and Pombo [50] is presented here, being the interested reader referred to the original reference for a detailed description of the methodology.

1.4.1 A General Formulation of a Clearance/Bushing Joint

A clearance/bushing joint constraining the relative motion between connected bodies requires the force penalization of the axial and radial displacements, axial misalignment and axial rotation described in Fig. 1.23. The joint reaction forces, here called also penalization forces, are applied in the bodies connected by the joint in the attachment points. The joint reaction forces are represented here as contact

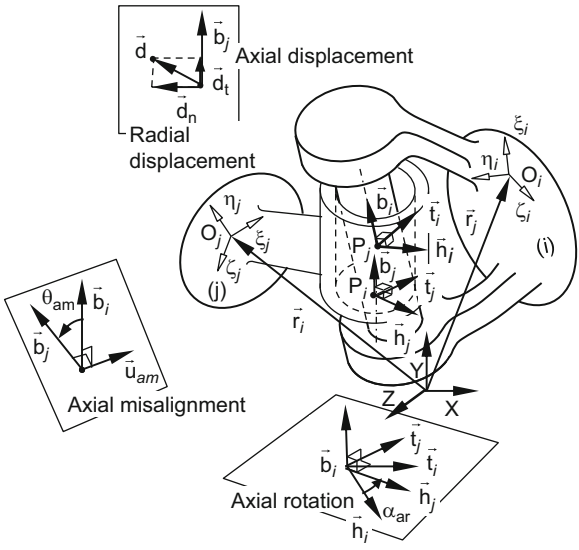

Fig. 1.23 Representation of a general clearance/bushing joint with the identification of specific relative motions required for its formulation

forces between the two bodies, using a methodology in line with those proposed by Ambrosio and Verissimo [48], for pure bushing joints, and by Flores et al. [47], for clearance joints.

To define the axial and radial displacements, axial misalignment and axial rotation, appearing in Fig. 1.23 let the distance vector $\mathbf{d}$ be decomposed into an axial displacement along vector $\mathbf{b}_i$, which specifies the joint axis in body j, defined as

$$\mathbf{d}_t = \left(\mathbf{d}^T \mathbf{b}_i\right) \mathbf{b}_i \tag{1.34}$$

and an orthogonal component, the radial displacement with respect to the joint axis, as

$$\mathbf{d}_n = \mathbf{d} - \mathbf{d}_t \tag{1.35}$$

The radial displacement, δ_n, and the radial direction, $\mathbf{u}_{rd}$, are

$$\delta_n = \sqrt{\mathbf{d}_n^T \mathbf{d}_n} \quad \text{and} \quad \mathbf{u}_{rd} = \mathbf{d}_n / \delta_n \tag{1.36}$$

The axial displacement, δ_t, and the radial direction vector, $\mathbf{u}_{ad}$, are

$$\delta_t = \sqrt{\mathbf{d}_t^T \mathbf{d}_t} \quad \text{and} \quad \mathbf{u}_{ad} = \mathbf{d}_t / \delta_t \tag{1.37}$$

The axial misalignment of the joint axis in bodies i and j is described by an angle θ_{am} measured about a vector $\mathbf{u}_{am}$ such that

$$\theta_{am} = \arcsin\left(\left|\tilde{\mathbf{b}}_i \ \mathbf{b}_j\right|\right) \quad \text{and} \quad \mathbf{u}_{am} = \tilde{\mathbf{b}}_i \ \mathbf{b}_j / \left|\tilde{\mathbf{b}}_i \ \mathbf{b}_j\right| \tag{1.38}$$

The skew-symmetric matrix of a vector $\mathbf{b}$ is denoted by $\tilde{\mathbf{b}}$. If the axial misalignment is null, i.e., $\left|\tilde{\mathbf{b}}_i \ \mathbf{b}_j\right| \approx 0$, Eq. (1.38) is not required because the conditions of alignment of the axis of the bearing and journal are fulfilled. The axial rotation of the bearing, with respect to the journal, is defined by the angle

$$\alpha_{ar} = arc \ \sin\left(\mathbf{h}_i^T \mathbf{t}_j\right) \tag{1.39}$$

The evaluation of the misalignments and relative displacements between bearing and journal involve the same vectors used to setup the perfect kinematic joints. From the point of view of the model construction this means that the same is used to setup perfect kinematic and clearance/bushing joints. The cylindrical clearance/bushing joint is obtained by penalizing of the radial displacement and the axial misalignment between bearing and journal by a penalization forces written as

$$\begin{aligned} \mathbf{f}_i^{(cyl)} &= \mathbf{f}_{cyl}\left(\delta_n, \dot{\delta}_n, \delta_t, \dot{\delta}_t, \theta_{am}, \dot{\theta}_{am}\right) \\ \mathbf{f}_j^{(cyl)} &= -\mathbf{f}_i^{(cyl)} \end{aligned} \tag{1.40}$$

The force constitutive equation $\mathbf{f}_{cyl}\left(\delta_n, \dot{\delta}_n, \delta_t, \dot{\delta}_t, \theta_{am}, \dot{\theta}_{am}\right)$ may involve the coupling of the relative displacements and misalignments. It also involves the clearance size, bearing and journal geometry and the material constitutive properties. For the complete definition of the cylindrical joint a penalization moment must be considered, written as

$$\begin{aligned} \mathbf{n}'^{(cyl)}_i &= \mathbf{n}_{cyl,i}\left(\delta_n, \dot{\delta}_n, \delta_t, \dot{\delta}_t, \theta_{am}, \dot{\theta}_{am}\right) \\ \mathbf{n}'^{(cyl)}_j &= \mathbf{n}_{cyl,j}\left(\delta_n, \dot{\delta}_n, \delta_t, \dot{\delta}_t, \theta_{am}, \dot{\theta}_{am}\right) \end{aligned} \tag{1.41}$$

A clearance/bushing, revolute joint requires the penalization forces and moments of the cylindrical joints and the penalization of the axial displacement as

$$\begin{aligned} \mathbf{f}^{(ad)}_i &= f_{ad}\left(\delta_t, \dot{\delta}_t\right)\mathbf{u}_{ad} \\ \mathbf{f}^{(ad)}_j &= -\mathbf{f}^{(ad)}_i \end{aligned} \tag{1.42}$$

The force relation $f_{ad}\left(\delta_t, \dot{\delta}_t\right)$ involves the axial displacement, its speed and the geometric and material characteristics of the joint.

The clearance/bushing translation joint besides the penalization forces and moments of the cylindrical joints also involves the penalization of the axial rotation, given by

$$\begin{aligned} \mathbf{n}'^{(ar)}_i &= f_{ar}\left(\alpha, \dot{\alpha}\right)\mathbf{A}^T_i\mathbf{b}_i \\ \mathbf{n}'^{(ar)}_j &= -\mathbf{A}^T_j\mathbf{A}_i\mathbf{n}'^{(ar)}_i \end{aligned} \tag{1.43}$$

where $f_{ar}\left(\alpha, \dot{\alpha}\right)$ is a nonlinear relation involving the axial rotation angle, its speed and the geometric and material characteristics of the joint.

The forces and moments of the clearance/bushing constitutive equations are applied in the bodies connected by the joint, i.e., on points P_i and P_j, in bodies i and j, respectively. The contribution of the clearance/bushing joints to the force vector of the bodies connected by one of those joints is

$$\begin{aligned} \mathbf{g}_i &= \begin{Bmatrix} \left(\mathbf{f}^{(cyl)}_i + \mathbf{f}^{(ad)}_i\right) \\ \mathbf{s}'^P_i\mathbf{A}^T_i\left(\mathbf{f}^{(cyl)}_i + \mathbf{f}^{(ad)}_i\right) + \mathbf{n}'^{(cyl)}_i + \mathbf{n}'^{(ar)}_i \end{Bmatrix}; \\ \mathbf{g}_j &= \begin{Bmatrix} \mathbf{f}^{(cyl)}_j + \mathbf{f}^{(ad)}_j \\ \mathbf{s}'^P_j\mathbf{A}^T_j\left(\mathbf{f}^{(cyl)}_j + \mathbf{f}^{(ad)}_j\right) + \mathbf{n}'^{(cyl)}_j + \mathbf{n}'^{(ar)}_j \end{Bmatrix} \end{aligned} \tag{1.44}$$

All forces and moments defined in Eqs. (1.40, 1.41, 1.42 and 1.43) involve the relative displacements and rotations and their time derivatives, for the evaluation of which the reader is directed to reference [48]. In the definition of the penalty moments, defined by Eqs. (1.41) and (1.43) the penalization of the axial displacement and axial rotation are decoupled from each other, and from the other relative

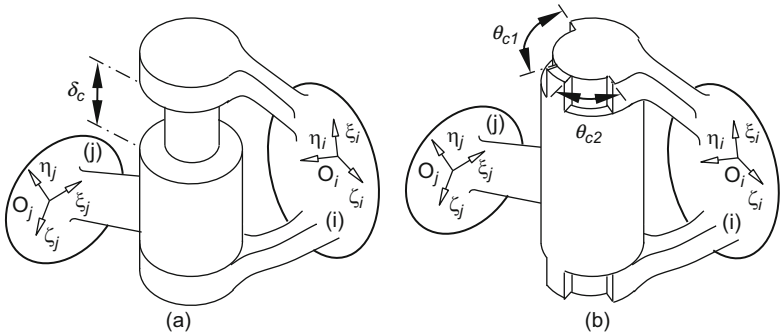

Fig. 1.24 Kinematic joints with limits in their range of motion: (**a**) cylindrical joint with limits on its translation displacement; (**b**) revolute joint with limits on its rotation range

motions. Depending on the material characteristics of the connected bodies, as in some biological applications or when involving some types of composite materials, some particular applications, the relative motion components may be coupled.

1.4.2 Joint Motion Limits

In practical applications the translation, cylindrical and revolute joints have limits on the relative motion between the two bodies, such as those illustrated in Fig. 1.24. The definition of the joint motion limits, for perfect kinematic joints or for clearance/bushing joints, are represented as a penalization of the joint motion after a given allowed range. From this point of view there is no difference in the methodology for the motion limit modeling in perfect kinematic or clearance/bushing joints. The penalization due to the joint stops is introduced in the force vector of the bodies that share the joint one of the relations defined by Eqs. (1.40, 1.41, 1.42 and 1.43), but considering the clearance size as the allowed range of motion.

For a perfect kinematic translation joint, with limits in the translation δ_c shown in Fig. 1.24a, the contributions to the system constraint equations and force vector

$$\begin{aligned} &\text{constraint equations}: \ \boldsymbol{\Phi}^{(trans,5)} = \mathbf{0} \\ &\text{force vector}: \quad \begin{cases} \mathbf{f}_i = \mathbf{f}_i^{(ad)}; \ \ \mathbf{f}_j = -\mathbf{f}_i^{(ad)} \\ \mathbf{n}'_i = \mathbf{A}_i^T \tilde{\mathbf{s}}_i^P \mathbf{f}_i; \ \ \mathbf{n}'_j = \mathbf{A}_j^T \tilde{\mathbf{s}}_j^P \mathbf{f}_j \end{cases} \end{aligned} \tag{1.45}$$

while for a clearance/bushing translation joint the kinematic constraint is substituted by the forces defined by Eqs. (1.40, 1.41, 1.42 and 1.43), applied as implied in Eq. (1.44).

For a perfect revolute joint with limits on its rotation given by $\theta_c = \theta_{c1} + \theta_{c2}$, as shown in Fig. 1.24b, the contributions for the constraint equations and force vector are

$$\begin{aligned} &\text{constraint equations : } \boldsymbol{\Phi}^{(rev,5)} = \mathbf{0} \\ &\text{force vector : } \begin{cases} \mathbf{f}_i = \mathbf{0}; \ \mathbf{f}_j = \mathbf{0} \\ \mathbf{n}'_i = \mathbf{n}'^{(ar)}_i; \ \mathbf{n}'_j = -\mathbf{A}_j^T \mathbf{A}_i \mathbf{n}'^{(ar)}_i \end{cases} \end{aligned} \tag{1.46}$$

For a clearance/bushing revolute joint the kinematic constraint, appearing in Eq. (1.46) is eliminated and, instead, the penalization forces characteristics of the joint, are used.

It should be noted that when the joint motion limits are hard stops the penalization of the relative motion is defined without involving the bushing in the penalization force constitutive relation. For joint limits defined with soft stops, such as the bounce stops in the vehicle suspensions, the penalization force model must take into account both bushing and hard contact, defined according to their physical characteristics.

1.4.3 Application to a 3D Slider-Crank Mechanism

The spatial slider-crank mechanism presented in Fig. 1.25 is part of the library of multibody benchmark problems [93]. The detailed slider-crank model and the initial conditions for the simulation are described in reference [50]. To demonstrate the use of clearance/bushing joints in the modeling of multibody systems several models are built either considering all its joints as perfect or including an imperfect revolute joint between ground and crank, being the clearance varied. The joints with a null clearances are still modeled as clearance/bushing joints, although it is expected that they still behave as perfect revolute joints, as those modelled with kinematic constraints.

The normal contact force model with hysteresis damping, expressed by Eq. (1.26), is used in the definition of the force penalization of the revolute joint.

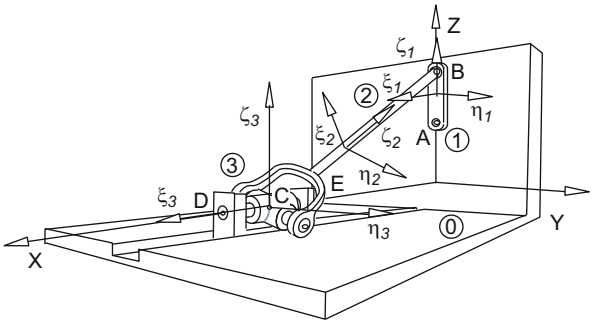

Fig. 1.25 Spatial slider-crank mechanism

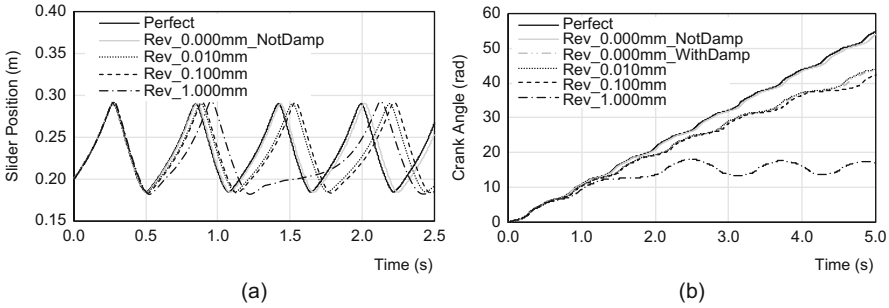

Fig. 1.26 Slider-crank model with revolute clearance joint: (**a**) slider position; (**b**) crank angle

The MUltiBOdy Dynamic analysis program MUBODyn [94] is used to develop the dynamic analyses of the models developed. The equations of motion of the system, together with the acceleration constraint equations, making a system of linear equations, are first solved for the unknown accelerations and Lagrange multipliers with a sparse matrix solver [96]. The velocities and accelerations are integrated numerically with the Gear multistep integrator [95]. The time stepping physical control procedure [69] is applied to detect the start of contact in all dynamic analyses for 5 s of simulation time.

The time histories of the slider block position and crank angle of the models are presented in Fig. 1.26. The results show that as the clearance in the revolute joint starts to increase, the time at which the slider reaches its end of stroke is increasingly delayed. For a clearance of 1 mm it is observed, in Fig. 1.26b, that the crank angle is unable to develop more than two revolutions, after which the crank ends up oscillating about its static equilibrium position. The effect of the energy dissipation due to the inclusion of the non-elastic restitution parameter in the contact force model is visible when comparing the responses of the models with a null clearance revolute joint with and without damping. The existence of the damping is responsible, just by itself, for the energy dissipation that forces the slider oscillation to increase the delay observed on reaching its end of stroke.

The joint reaction forces in the revolute joint are shown in Fig. 1.27. For the models with perfect revolute joints, modeled either as revolute kinematic constraints or as imperfect joints with null clearance, no oscillations in the reaction force are observed. As the clearance increases the joint reaction force of the revolute joint exhibits oscillations, mostly during the slider mid-stroke, being the amplitude of the force oscillations higher with the clearance size.

The presence of hysteresis damping in the normal contact model of the clearance joint eliminates the oscillations of the joint reaction forces. It has been observed in some cases that the friction forces, when present, also mitigate the oscillatory behavior observed in the contact joint [97]. The use of different numerical integrator schemes, with fixed or variable time steps or with internal damping can also mask, or emphasize, the oscillatory behavior observed.

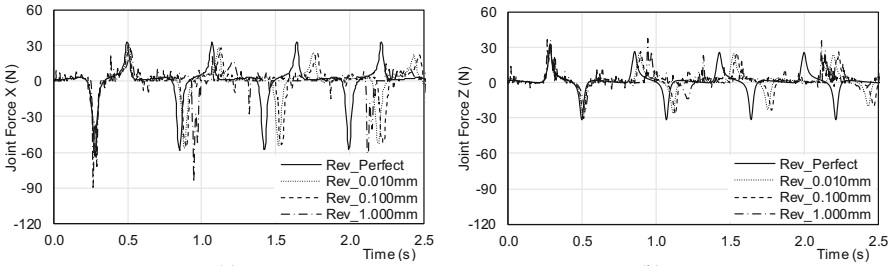

Fig. 1.27 Joint reaction force for the revolute joint slider crank models with perfect and with clearance revolute joint: (**a**) force component X; (**b**) force component Z

1.5 Highlights and Conclusions

This work identifies and discusses selected challenges on the formulation and application of multibody dynamics for important engineering systems. Important challenges, such as the computational geometry in kinematics and contact, formulation of complex kinematic joints, contact and impact in multibody dynamics, realistic modelling of common mechanical joints that exhibit clearances and local deformations, numerical issues associated with time integration or with nonlinear equations with physical inspired solution control, are just some of the topics which require a continued investigation for more advanced multibody systems. This work emphasized the importance of accurate and computational efficient developments in computational geometry to support other challenges in the modelling of multibody systems. The parametrization of curves and surfaces and their continuity not only need to fullfil the criteria associated to the specific application but also limit the numerical methods that can be applied in their solution. It has been observed that when the spatial curves, and surfaces, are used to setup kinematic constraints the minimum degree required for the polynomial description of the curve is that associated to the highest parametric derivative. However, when the same curve or surface is used in the context of contact mechanics the minimum continuity required depends on the solution method used for the contact detection. It has been shown that the use of nonlinear system of equations solvers, such as those implemented in the Matlab functions `fsolve` or `fmincon` only the parametric description of the curves or surfaces and their moving frame vectors, but are computationally more expensive than using the Newton-Raphson method. The drawback is that the Newton-Raphson method requires the derivatives of the parametric surfaces and associated vectors, putting higher demands on the degree of the parametric descriptions used. In any case, for large surfaces or long curves, eventually with a very fine discretization in terms of control nodes, it is not always possible, or efficient from the computational point of view, to keep them in memory. The use of look-up-tables, which allow that the contact search and the contact force evaluation to be done by linear interpolation of predefined nodes, avoid that complex operations

need to be carried online. The development of clearance/bushing joints in which the mechanical tolerances used in the construction of machines and mechanisms are reflected allow for the development of realistic models of multibody systems that would not be validated otherwise. The general formulation of this joints allows for the introduction of local deformation such as that exhibited by bushing joints. In all implementations of contact detection problems the numerical issues associated with time integration play a major role. It has been shown that adjusting the time-step of the time integrators, in particular those that use a variable time-step, is of fundamental importance. It is reinforced here the proposal that a physical control of the time-step, to prevent the initialization of a contact with a large interference between contacting surfaces, must be available complementary to the common mathematical control internal to these algorithms.

References

1. Hooker, W., Margulies, G.: The dynamical attitude equations for n-body satellite. J. Astronaut. Sci. **12**, 123–128 (1965)
2. Kane, T., Scher, M.: A dynamical explanation of the falling cat phenomenon. Int. J. Solids Struct. **5**(7), 663–670 (1969)
3. Kane, T., Scher, M.: Human self-rotation by means of limb movements. J. Biomech. **3**(1), 39–49 (1970)
4. Wittenburg, J.: The dynamics of systems of coupled rigid bodies. A new general formalism with applications. In: Grioli, G. (ed.) Stereodynamics. Edizione Cremonese, Roma (1971)
5. Wittenburg, J., Wolz, U., Schmidt, A.: MESA VERDE – a general-purpose program package for symbolical dynamics simulations of multibody systems. In: Schiehlen, W. (ed.) Multibody Systems Handbook. Springer, Heidelberg (1990)
6. Magnus, K.: Dynamics of Multibody Systems. Proceedings of the IUTAM Symposium, Munich, Germany, August 29 – September 3, 1977, Springer, Heidelberg (1978)
7. Haug, E.J. (ed.): Computer Aided Analysis and Optimization of Mechanical Systems Dynamics. Springer-Verlag, Heidelberg (1984)
8. Bianchi, G., Schiehlen, W. (eds.): Dynamics of Multibody Systems, Proceedings of the IUTAM/IFToMM Symposium, Udine, Italy, September 16–20, 1985. Springer, Heidelberg (1986)
9. Pereira, M., Ambrosio, J. (eds.): Computer-Aided Analysis of Rigid and Flexible Mechanical Systems, NATO Science Series E, vol. 268. Springer, Dordrecht (1994)
10. Schiehlen, W.: Multibody dynamics: roots and perspectives. Multi-body Syst. Dyn. **1**(2), 149–188 (1997)
11. Wittenburg, J.: Dynamics of Systems of Rigid Bodies. Teubner-Verlag, Wiesbaden (1977)
12. Nikravesh, P.E.: Computer-Aided Analysis of Mechanical Systems. Prentice-Hall, Englewood Cliffs (1988)
13. Kane, T., Levinson, D.: Dynamics: Theory and Applications. McGraw-Hill, San Francisco (1985)
14. Haug, E.: Computer Aided Kinematics and Dynamics of Mechanical Systems. Allyn and Bacon, Boston (1989)
15. Jalon, G., Bayo, E.: Kinematic and Dynamic Simulation of Multibody Systems: The Real-Time Challenge. Springer, Berlin (1994)
16. Erdman, A.G., Sandor, G.N.: Kineto-elastodynamics – a review of the state of the art and trends. Mech. Mach. Theory. **7**, 19–33 (1972)

17. Lowen, G.G., Chassapis, C.: Elastic behavior of linkages: an update. Mech. Mach. Theory. **21**, 33–42 (1986)
18. Thompson, B.S., Sung, G.N.: Survey of finite element techniques for mechanism design. Mech. Mach. Theory. **21**, 351–359 (1986)
19. Song, J.O., Haug, E.J.: Dynamic analysis of planar flexible mechanisms. Comput. Methods Appl. Mech. Eng. **24**, 359–381 (1980)
20. Shabana, A.: Dynamics of Multibody Systems. Wiley, New York (1989)
21. Shabana, A., Wehage, R.: A coordinate reduction technique for transient analysis of spatial structures with large angular rotations. J. Struct. Mech. **11**, 401–431 (1989)
22. Meirovitch, L., Nelson, H.D.: On the high-spin motion of a satellite containing elastic parts. J. Spacecr. Rocket. **3**, 1597–1602 (1966)
23. Modi, V., Suleman, A., Ng, A.: An approach to dynamics and control of orbiting flexible structures. Int. J. Numer. Methods Eng. **32**, 1727–1748 (1991)
24. Banerjee, A.K., Nagarajan, S.: Efficient simulation of large overall motion of nonlinearly elastic beams. In: Proceedings of ESA International Workshop on Advanced Mathematical Methods in the Dynamics of Flexible Bodies, ESA, Noordwijk, The Netherlands (1996)
25. Kane, T., Ryan, R., Banerjee, A.: Dynamics of a cantilever beam attached to a moving base. AIAA J. Guid. Control Dyn. **10**, 139–151 (1987)
26. Wallrapp, O., Schwertassek, R.: Representation of geometric stiffening in multibody system simulation. Int. J. Numer. Methods Eng. **32**, 1833–1850 (1991)
27. Geradin, M.: Advanced methods in flexible multibody dynamics: review of element formulations and reduction methods. In: Proceedings of ESA International Workshop on Advanced Mathematical Methods in the Dynamics of Flexible Bodies, ESA, Noordwijk, The Netherlands (1996)
28. Belytschko, T., Hsieh, B.J.: Nonlinear transient finite element analysis with convected coordinates. Int. J. Numer. Methods Eng. **7**, 255–271 (1973)
29. Simo, J.C., Vu-Quoc, L.: On the dynamics in space of rods undergoing large motions – a geometrically exact approach. Comp. Methods Appl. Mech. Eng. **66**, 125–161 (1988)
30. Bathe, K.-J., Bolourchi, S.: Large displacement analysis of three-dimensional beam structures. Int. J. Numer. Methods Eng. **14**, 961–986 (1979)
31. Cardona, A., Geradin, M.: A beam finite element non linear theory with finite rotations. Int. J. Numer. Methods Eng. **26**, 2403–2438 (1988)
32. Geradin, M., Cardona, A.: A modelling of superelements in mechanism analysis. Int. J. Numer. Methods Eng. **32**, 1565–1594 (1991)
33. Shabana, A.: Definition of the slopes and the finite element absolute nodal coordinate formulation. Multi-body Syst. Dyn. **1**, 339–348 (1997)
34. Ambrósio, J., Nikravesh, P.: Elastic-plastic deformations in multibody dynamics. Nonlinear Dyn. **3**, 85–104 (1992)
35. Ambrósio, J.: Dynamics of structures undergoing gross motion and nonlinear deformations: a multibody approach. Comput. Struct. **59**(6), 1001–1012 (1996)
36. Pereira, M.S., Ambrósio, J.: Crashworthiness analysis and design using rigid-flexible multibody dynamics with application to train vehicles. Int. J. Numer. Methods Eng. **40**(4), 655–687 (1997)
37. Shabana, A.: Flexible multibody dynamics: review of past and recent developments. Multibody Syst. Dyn. **1**(2), 189–222 (1997)
38. Geradin, M., Cardona, E.: Flexible Multibody Dynamics: A Finite Element Approach. Wiley, Chichester (2001)
39. Bauchau, O.: Flexible Multibody Dynamics. Springer, Dordrecht (2011)
40. Bremer, H.: Elastic Multibody Dynamics: A Direct Ritz Approach. Springer, Dordrecht (2008)
41. Gonzalez-Palacios, M., Angeles, J.: Cam Synthesis. Springer, Dordrecht (1993)
42. Gonzalez-Palacios, M., Angeles, J.: Synthesis of contact surfaces of spherical cam-oscillating roller-follower mechanisms. ASME J. Mech. Des. **116**(1), 315–319 (1994)
43. Pombo, J., Ambrósio, J.: General spatial curve joint for rail guided vehicles: kinematics and dynamics. Multi-body. Syst. Dyn. **9**(3), 237–264 (2003)

44. Ambrósio, J., Antunes, P., Pombo, J.: On the requirements of interpolating polynomials for path motion constraints. In: Kecskeméthy, A., Geu Flores, F. (eds.) Interdisciplinary Applications of Kinematics: Proceedings of the International Conference, pp. 179–197. Springer, Dordrecht (2015)
45. Tändl, M., Kecskemethy, A.: Singularity-free trajectory tracking with Frenet frames. In: Husty, M., Schroecker, H.-P. (eds.) Proceedings of the 1st Conference EuCoMeS. Innsbruck University Press, Obergurgl (2006)
46. Tändl, M.: Dynamic Simulation and Design of Roller Coaster Motion. VDI Verlag, Düsseldorf (2009)
47. Flores, P., Ambrósio, J., Pimenta Claro, J., Lankarani, H.: Kinematics and Dynamics of Multibody Systems with Imperfect Joints. Springer, Dordrecht (2008)
48. Ambrósio, J., Verissimo, P.: Improved bushing models for vehicle dynamics. Multi-body Syst. Dyn. **22**(4), 341–365 (2009)
49. Magalhaes, H., Ambrósio, J., Pombo, J.: Railway vehicle modelling for the vehicle-track interaction compatibility analysis. Proc. Inst. Mech. Eng. K J. Multi-body Dyn. **230**(3), 251–267 (2016)
50. Ambrósio, J., Pombo, J.: A unified formulation for mechanical joints with and without clearances/bushings and/or stops in the framework of multibody systems. Multi-body Syst. Dyn. **42**(3), 317–345 (2018)
51. Akhadkar, N., Acary, V., Brogliato, B.: Multibody systems with 3D revolute joints with clearances: an industrial case study with an experimental validation. Multi-body Syst. Dyn. **42**(3), 249–282 (2018)
52. Ambrósio, J.: Efficient kinematic joints descriptions for flexible multibody systems experiencing linear and non-linear deformations. Int. J. Numer. Methods Eng. **56**, 1771–1793 (2003)
53. Masarati, P., Morandini, M.: Intrinsic deformable joints. Multi-body Syst. Dyn. **23**, 361–386 (2010)
54. Cardona, A., Geradin, M., Doan, D.B.: Rigid and flexible joint modelling in multibody dynamics using finite elements. Comput. Methods Appl. Mech. Eng. **89**(1–3), 395–418 (1991)
55. Bae, D., Han, J., Choi, J.: An implementation method for constrained flexible multibody dynamics using virtual body and joint. Multi-body Syst. Dyn. **4**, 207–226 (2000)
56. Gonçalves, J., Ambrósio, J.: Advanced modeling of flexible multibody dynamics using virtual bodies. Comput. Assist. Mech. Eng. Sci. **9**(3), 373–390 (2002)
57. Mashayekhi, M., Kövecses, J.: A comparative study between the augmented Lagrangian method and the complementarity approach for modeling the contact problem. Multi-body Syst. Dyn. **40**(4), 327–345 (2017)
58. Blumentals, A., Brogliato, B., Bertails-Descoubes, F.: The contact problem in Lagrangian systems subject to bilateral and unilateral constraints, with or without sliding Coulomb's friction: a tutorial. Multi-body Syst. Dyn. **38**(1), 43–76 (2016)
59. Zhao, Z., Liu, C.: Contact constraints and dynamical equations in Lagrangian systems. Multibody Syst. Dyn. **38**(1), 77–99 (2016)
60. Flores, P., Leine, R., Glocker, C.: Modeling and analysis of planar rigid multibody systems with translational clearance joints based on the non-smooth dynamics approach. Multi-body Syst. Dyn. **23**(2), 165–190 (2010)
61. Kwak, S.D., Blankevoort, L., Ateshian, G.A.: A mathematical formulation for 3D quasi-static multibody models of diarthrodial joints. Comput. Methods Biomech. Biomed. Eng. **3**, 41–64 (2000)
62. Beia, Y., Fregly, B.J.: Multibody dynamic simulation of knee contact mechanics. Med. Eng. Phys. **26**(9), 777–789 (2004)
63. Machado, M., Flores, P., Pimenta Claro, J.C., Ambrósio, J., Silva, M., Completo, A., Lankarani, H.: Development of a planar multibody model of the human knee joint. Nonlinear Dyn. **60**(3), 459–478 (2010)
64. Anand, V.: Computer Graphics and Geometric Modeling for Engineers. Wiley, New York (1996)
65. Frenet, F.: Sur les courbes à double courbure. J. Math. Pures Appl. **17**, 437–447 (1852)

66. Machado, M., Flores, P., Ambrósio, J.: A lookup table-based approach for spatial analysis of contact problems. J. Comput. Nonlinear Dyn. **9**(1), 1–10 (2014)
67. Viegas, M., Ambrósio, J., Antunes, P., Magalhães, H.: Dynamics of a roller coaster vehicle. In: Spriyagin, M., Gordon, T., Cole, C., McSweeney, T. (eds.) Proceedings of the 25th International Symposium on Dynamics of Vehicles on Roads and Tracks (IAVSD 2017), Volume 2, pp. 551–556. CRC Press, Taylor and Francis, London (2017)
68. Kikuuwe, R., Brogliato, B.: A new representation of systems with frictional unilateral constraints and its Baumgarte-like relaxation. Multi-body Syst. Dyn. **39**(3), 267–290 (2017)
69. Flores, P., Ambrósio, J.: On the contact detection for contact-impact analysis in multibody systems. Multi-body Syst. Dyn. **24**(1), 103–122 (2010)
70. Haddouni, M., Acary, V., Garreau, S., Beley, J.-D., Brogliato, B.: Comparison of several formulations and integration methods for the resolution of DAEs formulations in event-driven simulation of nonsmooth frictionless multibody dynamics. Multi-body Syst. Dyn. **41**(3), 201–231 (2017)
71. Pombo, J., Ambrósio, J.: Application of a wheel–rail contact model to railway dynamics in small radius curved tracks. Multi-body Syst. Dyn. **19**(1), 91–114 (2008)
72. Pacejka, H.: Tyre and Vehicle Dynamics, 3rd edn. Butterworth-Heinemann, Amsterdam (2012)
73. Hirschberg, W., Rill, G., Weinfurter, H.: Tire model TMeasy. Veh. Syst. Dyn. **45**(1), 101–119 (2007)
74. Kalker, J.J.: Three-Dimensional Elastic Bodies in Rolling Contact. Springer, Dordrecht (1990)
75. Harris, T., Kotzalas, M.: Advanced Concepts of Bearing Technology. CRC Press, Boca Raton (2007)
76. Lankarani, H., Nikravesh, P.: Continuous contact force models for impact analysis in multibody systems. Nonlinear Dyn. **5**(2), 193–207 (1994)
77. Hunt, K.H., Grossley, F.R.E.: Coefficient of restitution interpreted as damping in vibroimpact. ASME J. Appl. Mech. **7**, 440–445 (1975)
78. Ambrósio, J.: Rigid and flexible multibody dynamics tools for the simulation of systems subjected to contact and impact conditions. Eur. J. Solids A Solids. **19**(S), 23–44 (2000)
79. Marques, F., Flores, P., Pimenta Claro, J., Lankarani, H.: A survey of several friction force models for dynamic analysis of multibody mechanical systems. Nonlinear Dyn. **86**(3), 1407–1443 (2016)
80. Bengisu, M.T., Akay, A.: Stability of friction-induced vibrations in multi-degree-of-freedom systems. J. Sound Vib. **171**, 557–570 (1994)
81. Kelley, C.T.: Iterative Methods for Linear and Nonlinear Equations. SIAM, Philadelphia (1995)
82. Gupta, P.K.: Advanced Dynamics of Rolling Elements. Springer, New York (1984)
83. Haines, D., Ollerton, E.: Contact stress distribution on elliptical contact surfaces subjected to radial and tangential forces. Proc. Inst. Mech. Eng. **177**, 95–114 (1963)
84. Magalhães, H., Madeira, J., Ambrósio, J., Pombo, J.: Railway vehicle performance optimization using virtual homologation. Veh. Syst. Dyn. **54**(9), 1177–1207 (2016)
85. Polach, O.: A fast wheel-rail forces calculation computer code. Veh. Syst Dyn. **33**, 782–739 (1999)
86. Ayasse, J., Chollet, H.: Determination of the wheel rail contact patch in semi-Hertzian conditions. Veh. Syst. Dyn. **43**, 161–172 (2005)
87. Sichani, M.S., Enblom, R., Berg, M.: A novel method to model wheel-rail normal contact in vehicle dynamics simulation. Veh. Syst. Dyn. **52**, 1752–1764 (2014)
88. Piotrowski, J., Liu, B., Bruni, S.: The Kalker book of tables for non-Hertzian contact of wheel and rail. Veh. Syst. Dyn. **55**(6), 875–901 (2017)
89. Escalona, J., Aceituno, J.: Modeling wheel-rail contact with pre-calculated lookup tables in arbitrary-geometry tracks with irregularities. In: ASME Proceedings of the 11th International Conference on Multibody Systems, Nonlinear Dynamics, and Control, Boston, Massachusetts, USA, August 2–5, Paper No. DETC2015-47306 (2015)
90. Zhang, J., Wang, Q.: Modeling and simulation of a frictional translational joint with a flexible slider and clearance. Multi-body Syst. Dyn. **38**(4), 367–389 (2016)

91. Pichler, F., Witteveen, W., Fischer, P.: A complete strategy for efficient and accurate multibody dynamics of flexible structures with large lap joints considering contact and friction. Multibody Syst. Dyn. **40**(4), 407–436 (2017)
92. Wang, G., Qi, Z., Wang, J.: A differential approach for modeling revolute clearance joints in planar rigid. Multi-body Syst. Dyn. **39**(4), 311–335 (2017)
93. Masoudi, R., Uchida, T., Vilela, D., Luaces, A., Cuadrado, J., McPhee, J.: A library of computational benchmark problems for the multibody dynamics community. In: Terze, Z. (ed.) Proceedings of ECCOMAS Multibody Dynamics., 1–4 July, pp. 1153–1162. University of Zagreb, Croatia (2013)
94. Ambrósio, J., Pombo, J.: MUltiBOdy Dynamic Analysis Program – MUBODyn: User's Manual, Technical Report IDMEC-CPM. Instituto de Engenharia Mecânica, Instituto Superior Técnico, University of Lisbon, Lisbon (2016)
95. Gear, G.: Numerical simulation of differential-algebraic equations. IEEE Trans. Circ Theory. **18**, 89–95 (1981)
96. Duff, I., Erisman, A., Reid, J.: Direct Methods for Sparse Matrices. Clarendon Press, Oxford (1986)
97. Ambrósio, J., Malça, C., Ramalho, A.: Planar roller chain drive dynamics using a cylindrical contact force model. Mech. Based Des. Struct. Mach. **44**(1–2), 109–122 (2015)